FCTUC DEPARTAMENTO DE ENGENHARIA CIVIL
FACULDADE DE CIÊNCIAS E TECNOLOGIA
UNIVERSIDADE DE COIMBRA

Fatigue Analysis of Bolted Connections with Adhesives

Thesis presented for the Master's Degree in Civil Engineering, Structural Mechanics

Author

Bruno Alexandre Silva Pedrosa

Supervisors

Professor Doutor Carlos Alberto da Silva Rebelo

Professora Doutora Maria Constança Simões Rigueiro

Coimbra, July, 2016

ACKNOWLEDGEMENTS

Although only one author is mentioned on the cover of this work several people have contributed for this project, directly or indirectly, in the previous months.

First of all, I want to demonstrate my special gratefulness to Professor José Correia for his tireless support, willingness and determination. For me, he is an example of dedication and commitment. During these months, he has showed a remarkable intelligence and passion for scientific research.

I want also to say thank you to Professor Carlos Rebelo and Professor Constança Rigueiro for the given support.

To Professor Sandra Carlos a special thanks for being constantly available and for the given support.

To my father, my mother and my brothers I send a special thanks for always being by my side. To Joana I want to send a special affection for always believing in me and for encourage me.

To my friends Ana Paula Forno, André Santos, David Valério, Diana Dias, João Duarte, João Vinhas, Pedro Patrício, Raquel Torra, Rodrigo Rodrigues, Rosário Silva e Sara Gouveia for their friendship and support I want to say thank you.

ABSTRACT

Taking into account both experimental and numerical approaches, there was the intention to examine if the introduction of structural adhesives on this kind of metallic connections contributes to an improvement in their fatigue strength.

Using injection bolts has been considered the most promising technique among others to implement on rehabilitation campaigns of old metallic structures.

Experimental results of two studies were analysed and then subjected to a statistical treatment in order to establish confident bands. Thus, for each case study a design curve was proposed. These curves were then compared to the code curves suggested in EC3-1-9. It was possible to understand that, in general, the code curves present conservative results, especially for high-cycle fatigue domains.

Regarding numerical approach, finite element models were developed with and without the application of adhesives in order to determine the stresses and strains field on its critical points. This implemented methodology allowed the definition of fatigue life predictions for crack initiation phase as well as understand the influence of the adhesive. Results have shown that using structural adhesives between the bolt shank and the plate hole walls leaded to an improvement in the fatigue strength on crack initiation phase.

For the fatigue crack propagation phase was assumed that adhesive will not produce any significant effect since at this stage only the mechanical properties of steel plates are relevant.

Aiming the definition of fatigue global prediction for the studied details, the obtained curves for crack initiation period was summed to the obtained curves for crack propagation period. Results have shown that fatigue crack propagation phase rules in low-cycle fatigue domains whereas fatigue crack initiation phase is dominant for high-cycle fatigue domains.

Keywords: Fatigue; Bolted Connections; Structural Strengthening; Structural Adhesives; Design Curves; Numerical modelling

RESUMO

Tendo em consideração quer uma abordagem experimental, quer uma abordagem numérica, procurou-se analisar se a introdução de adesivos estruturais nestas ligações metálicas contribui para uma melhoria da sua resistência à fadiga.

De entre as várias hipóteses existentes a implementar em campanhas de reabilitação de estruturas metálicas antigas, nomeadamente antigas pontes rebitadas, o uso de parafusos de injeção surge como a mais promissora.

Resultados experimentais de dois estudos foram submetidos a uma análise estatística visando estabelecer bandas de confiança. Assim, para cada caso de estudo foram propostas curvas de dimensionamento. Através da comparação entre estas curvas e as sugeridas na norma EC3-1-9 foi possível perceber que, na generalidade, estas últimas apresentam resultados conservadores, especialmente para elevado número de ciclos.

No que diz respeito à abordagem numérica das mesmas ligações, foram desenvolvidos modelos de elementos finitos com e sem a aplicação de adesivos com o intuito de determinar a história de tensões e deformações elastoplásticas nos pontos críticos. Esta metodologia permitiu estabelecer previsões da vida à fadiga na fase de iniciação, assim como analisar qual a contribuição do adesivo. Foi possível perceber que a introdução de adesivos estruturais entre o parafuso e as chapas origina uma melhoria na resistência à fadiga na fase de iniciação de fenda.

Para a fase de propagação da fenda de fadiga foi assumido que o adesivo não iria produzir qualquer influência uma vez que, nesta fase, apenas as propriedades mecânicas do aço usado nas chapas serão relevantes.

Com vista à obtenção de uma previsão global do comportamento à fadiga dos detalhes estudados, foram adicionadas as curvas obtidas para cada fase do fenómeno de fadiga. Os resultados mostraram que a fase de propagação da fenda governa para fadiga supercíclica enquanto a fase de iniciação da fenda é dominante para fadiga oligocíclica.

Palavras-chave: Fadiga; Ligações Aparafusadas; Reforço Estrutural; Adesivos Estruturais; Curvas de Dimensionamento; Modelação Numérica

CONTENTS

SYMBOLOGY

Latin Symbols

a	crack length
a_i	initial crack length
a_f	final crack length
Δa	crack increment
A, B	linear regression parameters
b	fatigue strength exponent
c	fatigue ductility exponent
C	material constant
C_p	friction parameter for preload calculations
da/dN	fatigue crack growth rate
d_b	bolt diameter
d_h	hole diameter
D_d	cumulative fatigue damage
E	Young's modulus
$f_{b,resin}$	bearing resistance of resin
$f_R\ (\Delta K)$	function of stress intensity factor that depends on stress ratio
F	applied load
$F_{p,C}$	applied preload on bolt
$F_{s,Rd,ser}$	design slip resistance at serviceability limit state
$\Delta F_{v,Sd,ser,max}$	maximum load range per bolt
ΔJ	strain energy release density
ΔJ_{th}	threshold of strain energy release density
k	number of tested specimens
κ_t	material constant
K	stress intensity factor
K'	cyclic hardening coefficient
K''	monotonic hardening coefficient
K^*	cyclic hardening coefficient for cyclic curve definition in local models based on energy
K_c	fracture toughness
K_{max}	maximum stress intensity factor
K_{min}	minimum stress intensity factor
K_t	stress concentration factor
ΔK	stress intensity factor range

$\overline{\Delta K}$	equivalent stress intensity factor range
ΔK_{th}	threshold of stress intensity factor range
m	slope of fatigue curve
M_p	applied torque on bolt
n'	cyclic hardening exponent
n''	monotonic hardening exponent
n^*	cyclic hardening exponent for cyclic curve definition in local models based on energy
n_{Ei}	number of cycles associated with the stress range $\gamma_{Ff}\Delta\sigma_i$
N	number of cycles
N_f	number of cycles in failure
$N_{f,j}$	number of cycles in failure for tested specimen j
N_i	number of cycles for crack initiation
N_P	number of cycles for crack propagation
N_{Ri}	endurance value (in cycles) for band i in the load spectrum
ΔN	increment on cycles
R	coefficient of correlation
R^2	coefficient of determination
R_ε	strain ratio
R_σ	stress ratio
S	standard deviation
S^2	variance
t	thickness of the plate
ΔT	temperature range
ΔW^E	elastic strain energy per cycle
ΔW^P	plastic strain energy per cycle
ΔW^t	total strain energy per cycle
ΔW_0^t	total strain energy per cycle corresponding to fatigue limit
X	independent variable
X_j	value of the independent variable for tested specimen j
$\bar{X}$	mean value of X_j
Y	dependent variable
Y_j	value of the dependent variable for tested specimen j
$\bar{Y}$	mean value of Y_j

Greek Symbols

α	integer number for statistical analysis
a_t	material constant
γ	curve fitting parameter

γ_{Ff}	partial safety factor for fatigue loads
γ_{Mf}	partial safety factor for fatigue strength
$\Delta\varepsilon$	strain range
$\Delta\varepsilon^*$	strain range for cyclic curve definition in local models based on energy
$\Delta\varepsilon^E$	elastic component of strain amplitude
$\Delta\varepsilon^P$	plastic component of strain amplitude
$\Delta\sigma$	stress range
$\Delta\sigma^*$	stress range for cyclic curve definition in local models based on energy
$\Delta\sigma_C$	reference value of the fatigue strength at 2 million cycles; detail category
$\Delta\sigma_D$	constant amplitude fatigue limit
$\Delta\sigma_i$	stress range for band i in the load spectrum
$\Delta\sigma_j$	stress range for tested specimen j
$\Delta\sigma_L$	cut-off limit
$\Delta\sigma_{loc}$	local stress range
$\Delta\sigma_R$	direct stress range
$\delta\sigma_0$	increase in the proportional stress due to non-Masing behaviour of the material
ε'_f	fatigue ductility coefficient
ε_a	strain amplitude
ε_{loc}	local strain
ε_{max}	maximum strain
ε_{med}	mean strain
ε_{min}	minimum strain
ρ^*	elementary material block size
σ	uniaxial tension
σ'_f	fatigue strength coefficient
σ_a	stress amplitude
σ_{loc}	local stress
$\sigma_{loc,med}$	local mean stress
σ_{max}	maximum stress
σ_{med}	mean stress
σ_{min}	minimum stress
σ_{nom}	nominal stress
σ_x	stress on x direction
$\sigma_{x,nom}$	nominal stress on x direction
$\sigma_{x,peak}$	peak stress on x direction

ACRONYMS

AASHTO	American Association of State Highway and Transportation Officials
ASCE	American Society of Civil Engineers
ASTM	American Society for Testing and Materials
BS	British Standard
CCS	Castillo and Fernández-Canteli
CT	Compact Tension
ECCS	European Convention for Constructional Steelwork
EC3-1-9	Eurocode 3 – Design of steel structures. Part 1-9: Fatigue
EFM	Elastoplastic Fracture Mechanics
EIFS	Equivalent Initial Flaw Size
FMA	Fracture Mechanics Approach
FRP	Fibre Reinforced Polymer
HSFG	High Strength Friction Grip
LEFM	Linear Elastic Fracture Mechanics
NDI	Non-destructive Inspection
RIBJ	Resin Injected Bolted Joints
RPT	Relative Penetration Tolerance
SSF	Stiffness Scale Factor
SWT	Smith, Watson and Topper
WWII	World War II

1 INTRODUCTION

1.1 Motivation

In the second half of the 19th and turn of the 20th century, new materials have widely spread throughout the world allowing for an exponential growth of metallic constructions, namely steel bridges, many of which are still in service nowadays (Akesson, 1994). In Portugal, there are also a large number of old steel bridges requiring maintenance and rehabilitation (Fernandes *et al* 2012). Through the years, this structures have been subjected to a constant increasing traffic levels, not only in terms of vehicle gross weight but also in terms of their frequencies. Consequently, governmental authorities need to implement and study innovative methods aiming to maintain their safety levels since their replacement in short period of time will be too costly. The most common evidences of damages in these structures are the presence of corroded metallic elements and cracks in structural details due to the fatigue phenomenon (Cavadas, 2008).

At the time that these structures were design, there was only a rough understanding on the fatigue phenomenon, since it only has been intensively investigated after the second half of the 20th century. Consequently, fatigue assessment of old riveted bridges has been a major concern (Larsson, 2009). In Figure 1.1 is illustrated an example of a typical fatigue crack found in structural elements of Eiffel bridge, in Viana do Castelo.

Figure 1.1 – Fatigue crack growing from a rivet hole (Jorge *et al*, 2006)

Different strategies can be implemented for repairing and strengthening operations of old steel riveted bridges. In order to preserve their original architecture, riveting might be used, however this process is no longer a common practice. The use of welding may not be appropriate since

old steels are characterized by their poor weldability properties. Another possibility is using high-strength friction grip (HSFG) bolts, but their good performance is dependent on the friction behaviour between the connected plates and on long term preload forces. Concerning the use of fitted bolts, their application requires an expensive preparation of the holes. Therefore, implement bolted connections with adhesives might be the most appropriate solution (De Jesus *et al*, 2010).

This technique has already been applied successfully in reparation of old bridges (ECCS Publication No. 79, 1994). For example, when was studied the rehabilitation of an old riveted steel bridge in Oranienburg, linking Netherlands to German, the decision was using injection bolts to connect new plates in corroded areas of its structural elements (Gresnigt *et al*, 2000). Even in Portugal, the use of resin-injected bolts has been reported (Mattes, 2007).

However, the fatigue behaviour of bolted connection with adhesives has not been widely studied. In literature, experimental campaigns in bolted connections with resin-injected bolts (De Jesus *et al*, 2010) were performed with reduced number of specimens which does not allow to implement a global characterization on the fatigue behaviour of this kind of connections. Furthermore, numerical simulations are also rare (Kortis, 2011).

1.2 Objectives

The present work aims at contributing to a better understanding of the fatigue behaviour of bolted connections with adhesives and stablish reliable prediction models.

In order to reproduce as close as possible the real situation of strengthening techniques using bolted connections with adhesives, an experimental campaign was prepared whose specimens connect new steel to old steel obtained from existing bridges under reparation. The main goal is to assess fatigue strength of bolted connections when using injected bolts in comparison to standard bolts. Although the specimen's preparation could be finished during the development of this thesis, it was not possible to carry out the experimental tests in time to be included in this document.

Nevertheless, the main works presented in literature concerning experimental researches on bolted connections with adhesives under fatigue loading were analysed. Through a statistical treatment of fatigue data, a design S-N curve was proposed in each case study. This proposed curve also served as comparison to the S-N curves suggested in EC3-1-9.

Furthermore, numerical simulations were performed. Parametric finite element models of bolted connections with and without adhesives were constructed aiming to define the range of stresses and strains presented on its critical locations. The obtained data was used in fatigue life

prediction models in order to determine the necessary number of load cycles needed for crack initiation. Fatigue crack propagation period was also analysed, in this case using the theory of Linear Elastic Fracture Mechanics (LEFM). The influence of using adhesives in bolted connections was studied in both fatigue crack initiation and propagation phases.

Finally, global predictions on the fatigue strength of the studied detail was proposed and compared with experimental data.

1.3 Organisation

The presented document is organized in 6 chapters including this one.

On chapter 2 is presented a general characterization on the fatigue phenomenon of metallic materials concerning two different phases: fatigue crack initiation and fatigue crack propagation. Furthermore, the most relevant fatigue life prediction models existing in available literature are described, namely prediction models based on global approaches, local approaches, using Fracture Mechanics concept and their combination.

Then, on chapter 3, the concept of resin-injected bolts is analysed along with their potential for use in structural strengthen operations. Experimental results of bolted connections with adhesives under fatigue loading conditions were analysed. Two case studies were summarized and fatigue data was presented in the form of S-N curves. The first case study performed by De Jesus *et al* (2010) focuses on comparison between bolted connection with resin-injected bolts and standard bolts in terms of their fatigue strength whereas the second case study, carried out by Albrecht *et al* (1984), concerns about the comparison between bolted connection with bonded plates and non-bonded plates, also regarding their fatigue strength. For each case study, a statistical analysis was implemented in order to propose fatigue design curves which were then compared the S-N curves proposed in EC3-1-9. Furthermore, there is also present on this chapter the main conclusions of fatigue tests on resin injected bolts joints with pultruded Fibre Reinforced Polymer (FRP) material.

Chapter 4 presents fatigue numerical analysis of steel connections using standard bolts and resin-injected bolts. Fatigue life prediction are presented for both crack initiation and propagation phases. The benefits of using adhesives will be analysed in both phases. Then, global predictions are also presented in order to validate fatigue experimental data.

On chapter 5 the main conclusions from experimental and numerical approaches are presented.

And finally, on chapter 6 are suggested future investigations on both numerical and experimental approaches concerning the fatigue analysis of bolted connections with adhesives.

2 FATIGUE AND FRACTURE OF MATERIALS

2.1 Introduction

Fatigue and fracture of materials started being a concern in the 19th century, when the German mining administrator, Wilhelm Albert, published the first known results about fatigue failure in metallic components. Furthermore, with the development of metallic materials and its use in civil engineering structures, specifically in highway and railway bridges, fatigue phenomena began to be documented more frequently (Schijve, 2004).

August Wöhler stood out for his engineering research on fatigue. He understood that a repeated load could induce a complete failure, even with a magnitude far below the static strength of a structure. He also introduced the concept of fatigue limit along with fatigue phenomenon characterization using stress-life curves, which became known as Wöhler curves or S-N curves. Later in the 20th century, investigations proved that repeated loads (service loads) can start a fatigue mechanism in the material, beginning from nucleation of micro-cracks, which can evolve with a crack growing process leading to complete failure (Schijve, 2004).

Fatigue prediction models began with Palmgren (in 1937) and Miner (in 1945) who proposed the linear damage accumulation theory, known as Miner's Rule. Later, Coffin (in 1945) and Mason (in 1953) performed scientific investigations in order to describe cyclic plastic behaviour of metallic materials leading to the empiric Coffin-Mason relation. Fracture Mechanics approaches, which comprise the fatigue crack propagation study, were developed by Griffith (in 1920) (Correia, 2014).

In the 50s, Irwin achieved an important progress showing that the stress level around the crack could be quantified using a scalar quantity named stress intensity factor. In 1961, Paris, Gomez and Anderson used this concept to develop a fatigue crack propagation law. Recently, new fatigue prediction models have emerged trying to overcome the weaknesses or disadvantages of previously proposed approaches, nonetheless there is yet no full understanding of the fatigue phenomenon, neither a general model capable of solving any fatigue problem (Correia, 2014).

A general characterization on the fatigue phenomenon is initially presented in this chapter, namely a description of the different phases in fatigue process. Cyclic stress cases are also analysed as well as the most relevant fatigue life prediction models within the scientific community.

2.2 General characterization on the fatigue phenomenon

2.2.1 Different phases of fatigue damage

Fatigue phenomenon normally starts at a microscopic scale, although it can evolve significantly and cause specimen failure or irreversible damage of structures. This fatigue behaviour needs to be properly acknowledged and the best way to do so is by dividing it in two parts: the crack initiation period and the crack growth period (Schijve, 2004).

This division is important because each phase of the fatigue phenomenon is influenced by different aspects. While some surface conditions, namely surface roughness (a texture indicator), do affect the crack initiation period, it has a negligible influence on the crack growth period. Therefore, fatigue prediction models are also distinct for these two periods. In fatigue prediction models for crack initiation, the stress concentration factor, K_t, is used: a parameter that characterizes the severity of stress distribution around a notch. Nevertheless, when the notch evolves into a crack, this parameter is meaningless. A crack differs from a notch specially in geometry: a notch typically has a circular or elliptical form and can be defined by two main axes. It turns into a crack since one axis becomes much bigger than the other. Consequently, to define crack growth period, stress intensity factor, K, is used, which characterizes the stress field around the crack (Schijve, 2004).

The definition of the fatigue limit can be expressed as the cyclic stress level below which fatigue failure does not occur. A schematic representation of the various steps of fatigue life and its important parameters is presented in Figure 2.1 (Schijve, 2004).

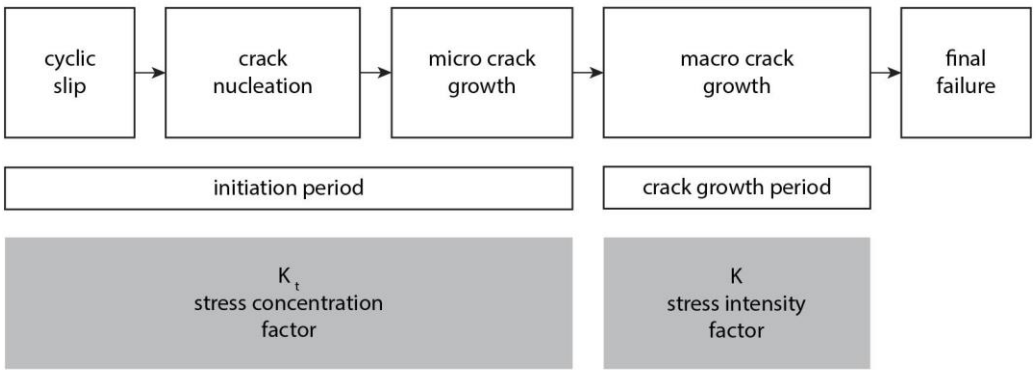

Figure 2.1 - Different phases of fatigue life and important factors (adapted from Schijve, 2004)

Fatigue life of a structural element is considered to be the total number of load cycles endured in the two processes mentioned before, N_f being N_i referred to the initiation period, and N_P, to the propagation period, as shown in the following equation (1).

$$N_f = N_i + N_P \quad (1)$$

2.2.2 Fatigue crack initiation period

Previous investigations on laboratory specimens have shown that invisible micro cracks remain in most part of the total fatigue life. At the moment those fatigue cracks become visible, only a small percentage remains of the total life of the material. However, in real structures such as ships, aircraft and bridges, this remaining life may be much longer than the investigations carried out in laboratory specimens (Schijve, 2004).

Fatigue crack initiation implies some amount of cyclic plastic deformation and it normally occurs at stress amplitudes below the yield stress of the material. Therewith, this plastic deformation is restricted to small and specific grains in the material. Those in the material surface are the most vulnerable due to the fact that the surrounding material is present on one side only. As a matter of fact, crack initiation period is mainly influenced by material surface conditions. Thus, stress concentration on the surface (due to a notch effect or some other geometric discontinuity), surface roughness or corrosion pits are aspects to take into account (Schijve, 2004).

Crack initiation period also includes initial micro-crack growth. Previous studies showed that it starts with a relatively high crack growth rate and then slows down or even stops due to material structural barriers (Schijve, 2004).

2.2.3 Fatigue crack growth period

The crack initiation period may cover a large percentage of the fatigue life under high-cycle fatigue, since the applied stress amplitude is just above the fatigue limit. Nonetheless, for large stress amplitudes, fatigue crack growth period can be a significant portion of the fatigue life. There is no way to define the transition from the initiation period to the crack growth period in quantitative terms because the transition depends on microstructural barriers (grain boundaries) that are not the same in all materials. However, it can be established that when micro crack growth has occurred away from the nucleation site, it is the beginning of the real crack growth period (Schijve, 2004).

At this stage, surface conditions are no longer relevant parameters, and crack growing resistance depends on the material as a bulk property. There is a general tendency in the crack growing process to develop in a direction perpendicular to the load (Schijve, 2004).

2.2.4 Cyclic stress cases

Within the scientific community focused on studying fatigue, it is widely accepted that fatigue damage is related to stresses or strains varying in time. Fatigue cyclic load can be divided in

three different categories: constant amplitude loading spectrums, variable amplitude loading spectrums defined by constant amplitude blocks and variable amplitude loading spectrums, randomly defined (Correia, 2008).

In order to characterize constant amplitude stress cycles, Figure 2.2 shows the different parameters that should be established, such as the maximum and minimum stresses, σ_{max} and σ_{min}, the stress range, $\Delta\sigma = \sigma_{max} - \sigma_{min}$, the stress amplitude, $\sigma_a = (\sigma_{max} - \sigma_{min})/2$, the mean stress, $\sigma_{med} = (\sigma_{max} + \sigma_{min})/2$ and the stress ratio, $R_\sigma = \sigma_{min}/\sigma_{max}$. The most common values for stress ratio are $R_\sigma = 0$ (pulsating load) and $R_\sigma = -1$ (alternating load).

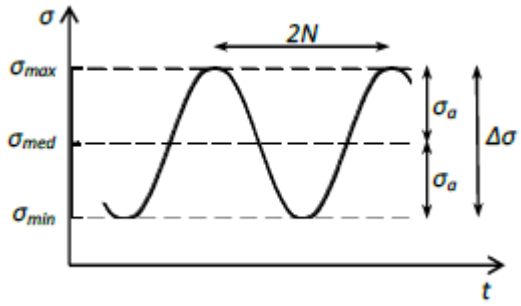

Figure 2.2 - Constant amplitude loading (Correia, 2014)

In the same way, similar expressions can be obtained if load magnitude is controlled by strain: for strain range $\Delta\varepsilon = \varepsilon_{max} - \varepsilon_{min}$, for strain amplitude $\varepsilon_a = (\varepsilon_{max} - \varepsilon_{min})/2$, for mean strain $\varepsilon_{med} = (\varepsilon_{max} + \varepsilon_{min})/2$ and for strain ratio $R_\varepsilon = \varepsilon_{min}/\varepsilon_{max}$ (Correia, 2008).

2.3 Fatigue Life Prediction Models

2.3.1 Introduction

This subchapter deals with the most relevant fatigue life prediction models existing in available literature. These models can be based on several distinct methods, such as global approaches, local approaches, using Fracture Mechanics concept and their combination.

Global analysis is directly dependent on the applied forces or in nominal stresses with the purpose of relating global failure of the components to loading (or stress) values. As far as local approaches are concerned, it aims to describe local damage phenomena using parameters obtained from stress or strain local analysis. Some prediction models make use of local approaches (especially strain-based models) together with a Fracture Mechanics approach in order to predict both fatigue crack initiation and crack propagation phases.

2.3.2 Global S-N models

Fatigue problems in structural elements are not easily understandable once several parameters, which are not always independent, command the structural response to cyclic loading.

Therefore, empirical procedures are commonly used to define and model fatigue response (Correia, 2014).

Experimental campaigns are usually performed to overcome this problem and establish a reliable prediction of fatigue behaviour. The typical way to represent fatigue damage for materials, mechanical components or structural details is to use S-N curves, also called Wöhler curves, which are based on constant amplitude loading. These curves relate stress amplitude to the number of cycles to failure, as shown in Figure 2.3 (a). These fatigue tests are performed on smooth un-notched specimens that make it almost impossible to establish the division between the crack initiation and propagation phases, hence the S-N curves usually represent only the total fatigue life of a specimen (Benden *et al*, 2009).

The fatigue strength of metallic materials is normally influenced by the value of mean stress, σ_{med}. Figure 2.3 (b) indicates that a higher mean stress will produce a lower S-N curve, however it is also noted that the effect of σ_{med} is not large, especially for high number of cycles (Schijve, 2004).

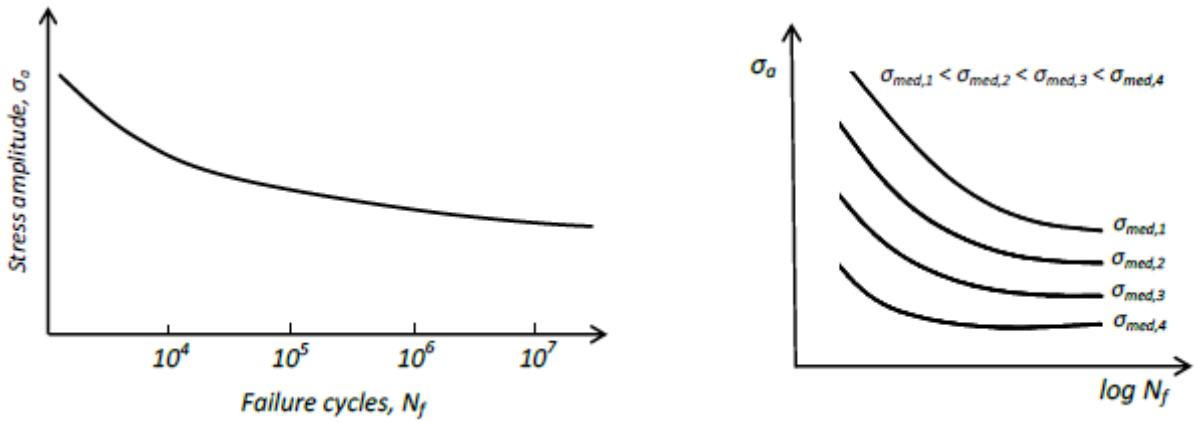

(a) (b)

Figure 2.3: (a) S-N diagram; (b) Influence of mean stress on S-N curves (Correia, 2014)

An S-N curve is obtained from experimental data of a number of fatigue tests performed at different stress levels. Figure 2.4 shows a schematic representation of such tests for un-notched specimens of a low alloy steel. As commonly used for S-N representations, these tests were executed with $\sigma_{med} = 0$ and, thus stress ratio is $R_\sigma = -1$. It is also preferable to adopt a logarithmic scale on both axes in order to establish a linear relation between $\log \sigma_a$ and $\log N$ for most results. This linear relation can be mathematically expressed by the Basquin relation as equation (2) demonstrates. The slope of the straight line is equal to $-1/m$ (Schijve, 2004).

$$\sigma_a^m N = constant \tag{2}$$

If maximum stress, σ_{max}, reaches the tensile strength of the material, the specimen will obviously fail in the first cycle as in a tensile test, thus the upper limit of S-N curves is

established by the tensile strength of the material. It may also present a flat zone for large number of cycles representing a distinct stress level below which fatigue failure will not occur. Between these limits, two regions may be defined in S-N curves. While fatigue failure at high stress amplitudes with corresponding short lives is called low-cycle fatigue, low stress amplitudes applied for a long number of cycles is referred to as high-cycle fatigue. There is no way to define in which number of cycles the transition between these two regions takes place, however their main difference is that low-cycle fatigue is associated with plastic deformation in every cycle and high-cycle fatigue is more related to elastic behaviour (Schijve, 2004).

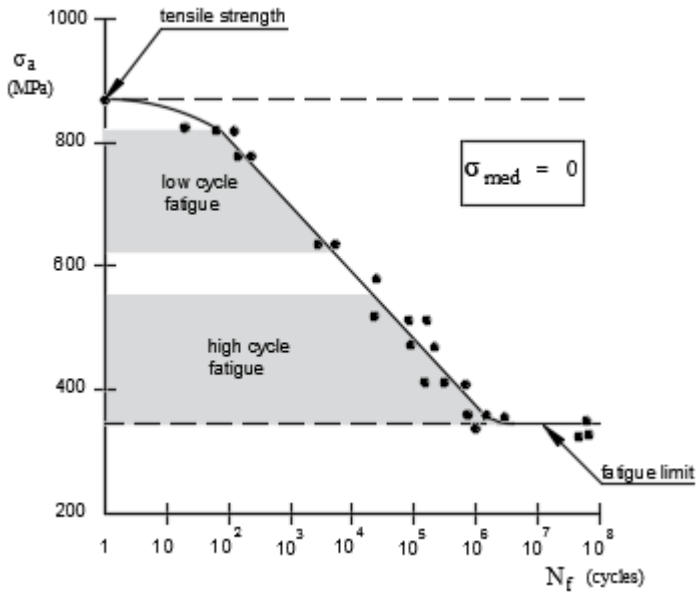

Figure 2.4 – S-N scheme of a low alloy steel (adapted from Schijve, 2004)

A given S-N curve is only valid for the specific conditions under which it was tested. This means that to extrapolate the results, the effects of several factors that influence an S-N curve must be properly acknowledged. These factors include member geometry, chemical environment, cyclic frequency, temperature, residual stress and mean stress (Benden *et al*, 2009).

In order to determine the remaining fatigue life of civil engineering structures, a detailed study needs to be performed on its critical components. The treatment of fatigue life in structural details is described by design rules of several European standards, such as, NP EN 1993-1-9:2010 (EC3-1-9) and BS 5400-10:1980. However, in what concerns fatigue design rules of resin injected bolted joints (RIBJ), only EC3-1-9 explicitly refers the S-N curve to be used. It presents a set of fatigue strength curves for direct stress ranges, each defined by its detail category (stress range, $\Delta\sigma_C$, at two million cycles), as Figure 2.5 shows. Table 2.2 summarizes the detail categories assigned for each type of RIBJ.

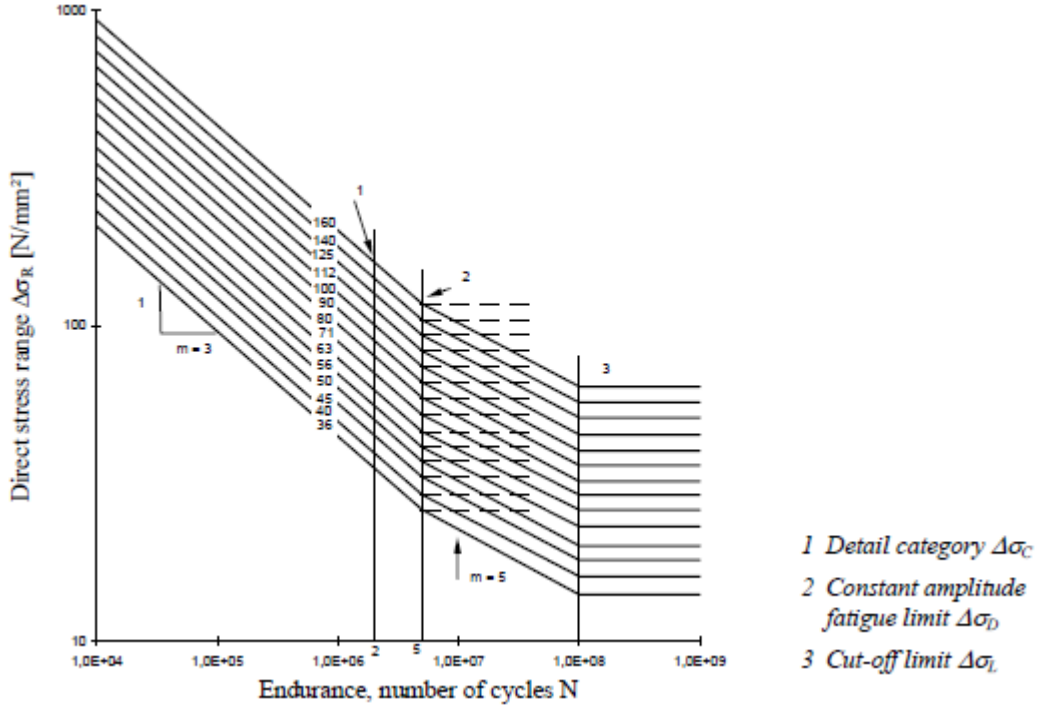

Figure 2.5 – Fatigue strength curves for direct stress ranges (EC3-1-9)

	Type of connection					
Detail Category	Symmetrical	Preloaded	Non Preloaded	Double shear	Single shear	$\Delta\sigma$ calculated on
112	x	x		x		gross cross-section
90			x	x		net cross-section
90		x			x	gross cross-section
80			x		x	net cross-section

Table 2.2 – Detail categories for RIBJ

In 1994, the European Convention for Constructional Steelwork (ECCS) published a document called *European Recommendations for Bolted Connections with Injection Bolts*. Practical guidelines for design are presented in order to relate load spectra to the strength capacity of the joint. Concerning non-preloaded connections, fatigue verifications must be implemented in three different fields: net section of the connected plates, shear of the bolt and resin. For the first two fields, a fatigue strength curve is defined (detail category 112 and detail category 100, respectively) based on EC3-1-9. For the resin field, the detail category follows from fatigue tests on RIBJ performed with different bearing stress ranges (0.90, 0.60 and 0.30) of the characteristic bearing resistance of the resin, $f_{b,resin}$, (obtained from static creep tests). Then, with applied stress range, $\Delta\sigma_i$, properly increased by the partial factor for fatigue loads, γ_{Ff}, and fatigue strength values acquired from fatigue strength curves divided by the partial safety factor for fatigue strength, γ_{Mf}, the endurance value (in cycles), N_{Ri}, for each band in the load spectrum is obtained. Cumulative damage, D_d, during the design life should be calculated from equation (3) where n_{Ei} is the number of cycles associated with the stress range $\gamma_{Ff}\Delta\sigma_i$ for band

i in the load spectrum. This fatigue assessment based on damage accumulation should meet the criterion: $D_d \leq 1.0$. The partial safety factors for fatigue loads and fatigue strength mentioned before are obtained from EC3-1-9.

$$D_d = \sum_i^n \frac{n_{Ei}}{N_{Ri}} \tag{3}$$

Regarding preloaded connections, this ECCS Recommendation lists two field regions to be verified: gross section of connected plates and load range per bolt. The procedure for the first field (detail category 112) is similar to that stated previously for non-preloaded connections, but to analyse the load range per bolt, equation (4) must be followed. $\Delta F_{v,Sd,ser,max}$ refers to the maximum applied load range per bolt and $F_{s,Rd,ser}$ is the design slip resistance per bolt, both determined at serviceability limit state (ECCS Publication No. 79, 1994).

$$\frac{\gamma_{Ff} \ \Delta F_{v,Sd,ser,max}}{2 \ F_{s,Rd,ser} \ / \ \gamma_{Mf}} \leq 1.0 \tag{4}$$

2.3.3 Local models

2.3.3.1 Introduction

The local approaches focus particularly on crack initiation period and they use fatigue damage parameters to correlate fatigue test results. Predictions on fatigue life can be implemented using different fatigue damage parameters, such as stress, strain and energy. This leads to the division of local approaches into three categories, *i.e.*, stress-based, strain-based and energy-based methods. In the following paragraphs several models proposed for each category are described.

2.3.3.2 Local models based on stresses

Local models based on stresses are characterized by establishing predictions on fatigue life (number of cycles to failure) using alternating stress amplitude. A way to express this relation is using S-N curves grounded on empirical formulas derived from experimental data. This stress-life model is best suited for high cycle fatigue, as under low cycle fatigue, stress-strain relation becomes nonlinear (Correia, 2014).

If stress amplitude, $\Delta\sigma/2$, and fatigue life, N_f, are both expressed on a logarithmic scale, a similar relation to S-N curves can be determined by using a straight line to represent the obtained data. Thus, in Basquin (1910) and equation (5) was proposed, where σ'_f is the fatigue strength coefficient and b is the fatigue strength exponent.

$$\frac{\Delta\sigma}{2} = \sigma'_f \left(2N_f\right)^b \quad (5)$$

In the former equation mean stress is assumed to be zero. Although for welded details this assumed fact is correct, in cases of non-welded details, the effect of stress level must be accounted for in fatigue life calculations. Consequently, Morrow (1965) proposed a correction to account for the mean stress effect (6) where σ_{med} is mean stress.

$$\frac{\Delta\sigma}{2} = \left(\sigma'_f - \sigma_{med}\right)\left(2N_f\right)^b \quad (6)$$

2.3.3.3 Local models based on strains

Local models based on strains are widely used in fatigue analysis, especially for calculation of fatigue crack initiation. These models differ from the previous ones because they take into account the plastic deformation that may occur in specific areas where fatigue crack initiates. The strain-based models consider that the material that surrounds highly strained areas (at a geometric discontinuity, for example) behaves in a similar way to the material in a smooth specimen, tested under cyclic strain controlled loading. Fatigue tests under strain-controlled conditions can be performed following the recommendations of the ASTM E606 standard (Correia, 2014).

Instead of using S-N curves, like in local models based on stresses, strain-based models are based on strain *versus* life curves together with cyclic stress *versus* strain curve of the material. Therewith, the coefficients and exponents that define theses curves need to be determined. At the time this method was developed, no sufficient fatigue data was available to quantify the fatigue properties of many engineering metals, thus various empirical equations were proposed to correlate fatigue properties to tensile properties. However, nowadays there is no need to use these empirical equations, given the abundance of data characterizing fatigue properties of numerous engineering materials (Correia, 2014).

The typical way to express strain-life data is to use the superposition of Coffin (1954) and Manson (1954) relation with Basquin (1910) relation leading to the recognized Morrow's equation (1965). The relation proposed by Coffin (1954) and Manson (1954), expressed in equation (7), is more capable of representing low-cycle fatigue data, considering that it relates the plastic component of strain amplitude, $\Delta\varepsilon^P/2$, with the number of cycles to failure, N_f. Parameters ε'_f and c are, respectively, fatigue ductility coefficient and exponent, both determined experimentally.

$$\frac{\Delta\varepsilon^P}{2} = \varepsilon'_f \left(2N_f\right)^c \quad (7)$$

In order to extended the Coffin (19549) and Manson (1954) relation to high-cycle fatigue domains, the relation proposed by Basquin (1910) can be used. Therefore, equation (8) expresses the relation between elastic strain amplitude, $\Delta\varepsilon^E/2$, and the number of cycles to failure, N_f, where σ'_f is the fatigue strength coefficient, b is the fatigue strength exponent and E is Young's modulus.

$$\frac{\Delta\varepsilon^E}{2} = \frac{\sigma'_f}{E}\left(2N_f\right)^b \tag{8}$$

As illustrated in Figure 2.6, the number of cycles (or reversals) corresponding to the transition between low and high cycle fatigue regimes is established when the total strain amplitude is composed of equal components of elastic and plastic strain amplitudes. Therefore, while lives below this transition value are ruled by ductility properties, above it, strength properties rule (De Jesus *et al*, 2010). Morrow (1965) suggested the algebraic sum of the two previous equations, as equation (9) shows, in order to obtain a more general equation, valid for both low and high fatigue regimes.

$$\frac{\Delta\varepsilon}{2} = \frac{\Delta\varepsilon^E}{2} + \frac{\Delta\varepsilon^P}{2} = \frac{\sigma'_f}{E}\left(2N_f\right)^b + \varepsilon'_f\left(2N_f\right)^c \tag{9}$$

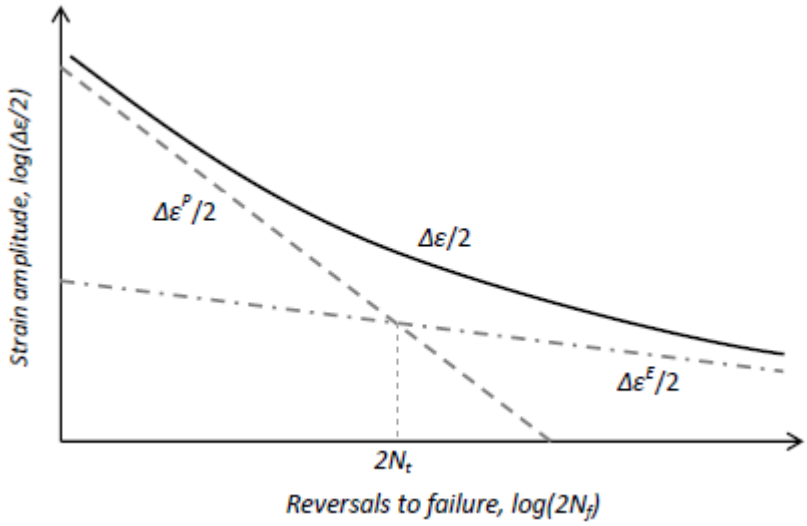

Figure 2.6 – Schematic representation of elastic, plastic and total strain amplitudes *versus* reversals to failure (Correia, 2014)

Fatigue tests performed in engineering metals usually show a cyclic hardening or softening firstly and then a stable condition is reached (Correia, 2014). At this stage, stress *versus* strain curve can be defined by the Ramberg-Osgood (1943) equation (10), where E is Young's modulus, K' is the cyclic strength coefficient and n' is the cyclic strain-hardening exponent.

$$\frac{\Delta\varepsilon}{2} = \frac{\Delta\varepsilon^E}{2} + \frac{\Delta\varepsilon^P}{2} = \frac{\frac{\Delta\sigma}{2}}{E} + \left(\frac{\frac{\Delta\sigma}{2}}{K'}\right)^{\frac{1}{n'}} \tag{10}$$

The cyclic curve can also be used to analyse whether the material presents a Masing behaviour. With the superposition of several stabilized hysteresis loops with the lower tips coincident at the origin of the graphs, if the ascending branches of the hysteresis cycles can be described by the cyclic stress-strain curve, equation (10), magnified by a factor of two, then the material has a Masing behaviour, as Figure 2.7 (a) shows. Most steel with carbon has a non-Masing behaviour, Figure 2.7 (b) (Correia, 2008).

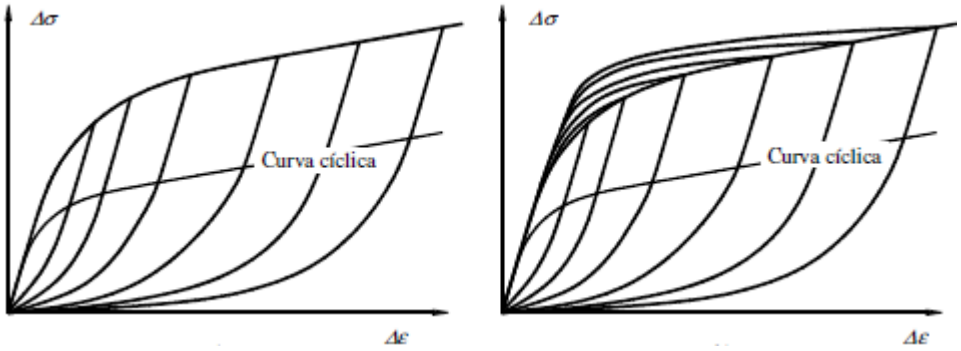

(a) (b)

Figure 2.7 – Typical hysteresis loops: (a) Masing behaviour; (b) Non-Masing behaviour (Silva, 2009)

As described for local models based on stresses, mean stress effect can be corrected by strain-based models. This correction can be performed by the Smith, Watson and Topper (SWT) (1970) model that provides good results for numerous engineering materials. It considers that the fatigue life of any level of mean stress is related to the product of the maximum stress, σ_{max}, and strain amplitude, Δε/2 as expressed in (11).

$$\sigma_{max}\frac{\Delta\varepsilon}{2} = \frac{\left(\sigma'_f\right)^2}{E}\left(2N_f\right)^{2b} + \sigma'_f\varepsilon'_f\left(2N_f\right)^{b+c} \tag{11}$$

2.3.3.4 Local models based on energy

Previous research on the fatigue damage process has confirmed that strain energy is dissipated during plastic deformations at microscopic level. It is precisely this energy parameter that is used to characterize fatigue in local models based on energy. They are able to model both high and low cycle fatigue and they do not depend on the specimen's geometry. These advantages facilitate the analysis of fatigue data from different laboratories around the world. Despite being developed in the last two decades and still not widely used, these models have a positive position within the scientific community (Correia, 2014).

The total absorbed energy, until fatigue failure has occurred, is assumed to be related to the endured number of cycles. On the other hand, fatigue damage arising in each cycle is assumed to be associated with the area under the hysteresis loop of the stress *versus* the strain curve obtained during cyclic loading. The dissipated energy can be measured in different ways, such as plastic strain energy per cycle, ΔW^P, and plastic plus elastic strain energy per cycle, ΔW^t. The first criterion is suitable when plastic strains are large but not recommended for small strain magnitude like in high cycle fatigue due to the fact that plastic strain energy is very small and difficult to be measured accurately. As for the ΔW^t criterion, it is believed to be more suitable for deformation controlled situations and it takes the mean stress effect into account (Kujawski, 1989).

Figure 2.8 presents a stable hysteresis loop as a cyclic response of a material when subjected to a constant strain range of $\Delta\varepsilon$. The absorbed plastic strain energy per cycle, ΔW^P, is the area inside the hysteresis loop (area OABCO in Figure 2.8). When a Masing behaviour is present, it can be calculated with equation (12) whereas for non-Masing behaviour equation (13) should be used. Parameter n' is the cyclic hardening exponent previously referred to in equation (10). For non-Masing behaviour, a "master curve", different from the cyclic curve, needs to be defined changing the involved parameters, such as $\Delta\varepsilon$, $\Delta\sigma$, K' and n' for $\Delta\varepsilon^*$, $\Delta\sigma^*$, K^* and n^*. This new curve is obtained from matching upper branches of the hysteresis loops through translating each loop along its linear response portion. In equation (13), $\delta\sigma_0$ is the increase in the proportional stress due to non-Masing behaviour of the material, and can be obtained from equation (14) (Kujawski, 1989).

$$\Delta W^P = \frac{1-n'}{1+n'}\Delta\sigma\Delta\varepsilon^P \tag{12}$$

$$\Delta W^P = \frac{1-n^*}{1+n^*}(\Delta\sigma - \delta\sigma_0)\Delta\varepsilon^P + \delta\sigma_0\Delta\varepsilon^P \tag{13}$$

$$\delta\sigma_0 = \Delta\sigma - \Delta\sigma^* = \Delta\sigma - 2K^*\left(\frac{\Delta\varepsilon^P}{2}\right)^{n^*} \tag{14}$$

Regarding the linear elastic strain energy, ΔW^E, it is obtained from the area BCDEB from Figure 2.8, and it is mathematically expressed by equation (15).

$$\Delta W^E = \frac{1}{2}\Delta\sigma\Delta\varepsilon^E \tag{15}$$

Consequently, the total cyclic strain energy is calculated as the sum of both areas mentioned before, as equation (16) shows.

$$\Delta W^t = \frac{1}{2}\Delta W^P + \frac{1}{2}\Delta\sigma\Delta\varepsilon^E \tag{16}$$

A fatigue failure criterion based on the total strain energy at half-life was developed by Ellyin and Kujawski (1986) in order to predict fatigue lives in both low and high cycle fatigue regions. The proposed power law is presented in equation (17) where $a_t < 0$ and $\kappa_t > 0$ are constants determined through the best fit given the experimental data obtained, N_f is the number of cycles to failure and ΔW_0^t is the total strain energy range, ΔW^t, corresponding to the fatigue limit.

$$\Delta W^t = \kappa_t\left(2N_f\right)^{\alpha_t} + \Delta W_0^t \tag{17}$$

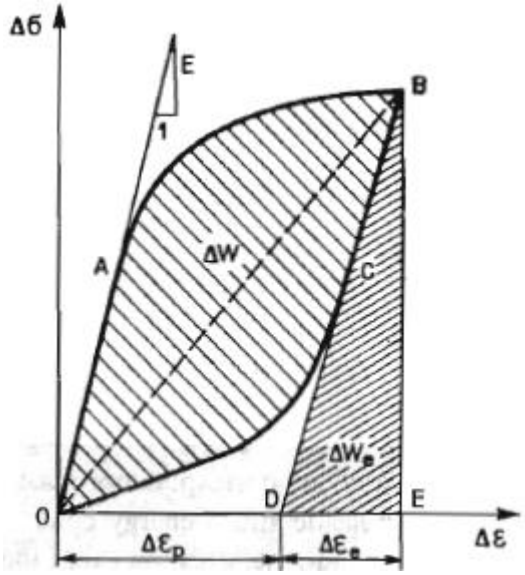

Figure 2.8 – Energy components extracted from a stable hysteresis loop (Kujawski, 1989)

2.3.4 Models based on Fracture Mechanics

2.3.4.1 Introduction

Fracture Mechanics deals with fracture phenomena, namely the combination between the mechanics of cracked bodies and its mechanical properties. This concept was established when some disasters occurred during World War II (WWII) with the appearance of fractures in ships and aircrafts. Failures occurred primarily when rivets were replaced by welded construction in materials with poor weldability properties leading to stress concentration. Nearly 14% of ships built during WWII disclosed serious fractures. Investigations on The Comets accidents in 1954 boosted significant progresses on the understanding of fracture and fatigue (Ribeiro *et al*, 2011).

In order to estimate the current fatigue resistance and the remaining fatigue life of a structure using traditional calculation, it is essential to analyse load history in terms of accumulated damage in the past. However, in most cases, especially in bridges, load history is not reported.

Consequently, if a crack is found and the load spectrum analysis is unapproachable, new methods can be applied, such as the Fracture Mechanics Approach (FMA) (Helmerich *et al*, 2007).

In order to better understand FMA, a previous analysis is performed on fatigue crack growth phenomenon as Fracture Mechanics based models are essentially fatigue crack growth prediction models.

2.3.4.2 Fatigue crack growth analysis

Fatigue crack growth rate can be analysed by specific tests performed with indications of ASTM standard E647-99:1999. It establishes the geometry of Compact Tension specimens – CT specimens (see Figure 2.9 (a)), namely the length of crack "a", and crack growth is recorded during the fatigue test by periodic observations. Obviously, the simplest way to present the experimental data is relating crack length data plotted as a function of the number of cycles, as presented in Figure 2.9 (b). It displays results from two different levels of stress amplitude, σ_a, both of them starting at the same initial crack length, a_i. Crack growth rate, da/dN is the slope of a crack growth curve, and it can be expressed in meters per cycle or some other useful unit (Schijve, 2004).

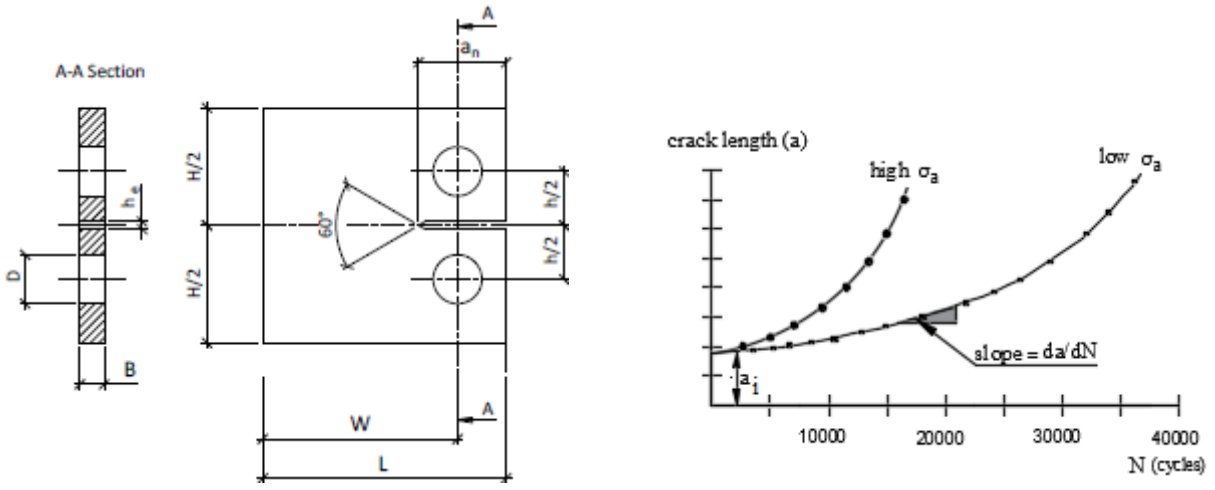

(a) (b)

Figure 2.9: (a) CT specimen geometry (ASTM E647-99, 1999); (b) Crack length as a function of the number of cycles (adapted from Schijve, 2004)

Moreover, Figure 2.10 presents crack propagation rate for high and low σ_a, as a function of crack length and an overlapping zone between these two curves can be observed. This fact means that similar crack growth rate occurs in the two tests, even though at different values of crack length.

Due to this similarity in crack growth rate, in Paris *et al* (1961) was developed the similarity principle based on stress intensity factor, K. This parameter indicates the severity of stress

distribution around the tip of a crack. The same way that cyclic stress varies between σ_{max} and σ_{min}, the corresponding stress intensity factor varies between K_{max} and K_{min}. Thus, the same stress ratio, R_σ, is obtained from cyclic stress and from the cyclic K values as shown in (18) (Schijve, 2004).

$$R_\sigma = \frac{\sigma_{min}}{\sigma_{max}} = \frac{K_{min}}{K_{max}} \tag{18}$$

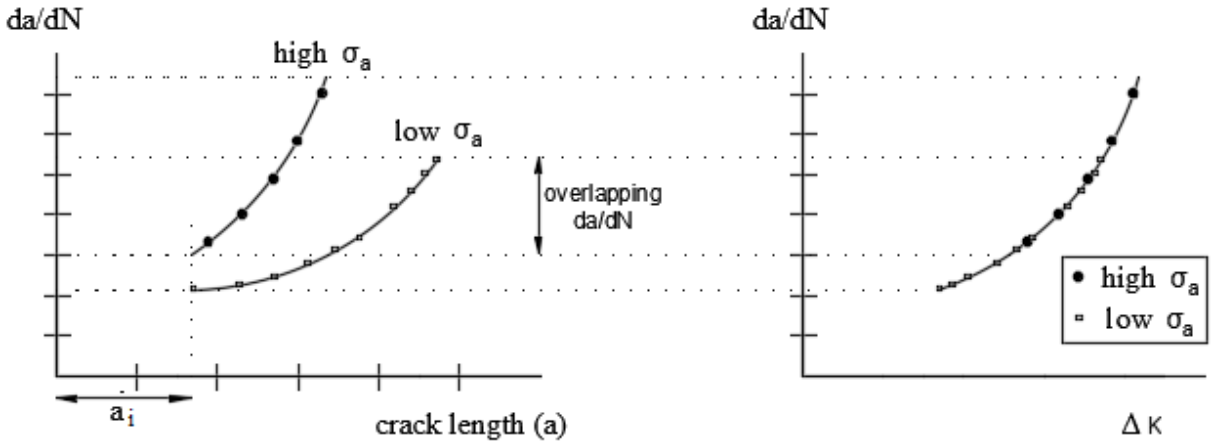

Figure 2.10 – Fatigue crack propagation at high and low σ_a (adapted from Schijve, 2004)

According to this similarity concept, crack growth rate must be a function of K_{min} and K_{max}. Since cyclic K values can also be defined by the stress intensity factor range, $\Delta K = K_{max} - K_{min}$, the relation between the stress intensity factor at an existing crack tip and crack advance under cyclic loading can be expressed by equation (19), where f_R is a function of stress intensity factor range that depends on stress ratio. This relation characterizes the crack growth resistance of a material. It has some limitations because the similarity principle only states that crack extension, Δa, in similar ΔK cycles should be the same. This principle does not imply anything about fatigue crack mechanism and it does not indicate how much crack extension should occur in a ΔK cycle (Schijve, 2004).

$$\frac{da}{dN} = f_R\,(\Delta K) \tag{19}$$

Figure 2.11 presents a schematic representation of the three fatigue crack growth regions in a double log scale. It shows two vertical asymptotes. The one on the left, at $\Delta K = \Delta K_{th}$, indicates that ΔK values below this threshold level are too low to cause macro crack growth while the right asymptote occurs for a ΔK cycle with $K_{max} = K_c$. It is a critical value for K_{max} which leads to complete failure of the specimen. These three regions can be named as: I – the threshold ΔK-region; II – the Paris ΔK-region; III - the stable tearing crack growth region (Schijve, 2004).

In an experimental campaign, ΔK must be decreased until zero crack growth is obtained and the lowest value reached is the threshold level, ΔK_{th}. Evidence has shown that ΔK_{th} is not a single material constant because it depends on stress ratio. Furthermore, this region is largely influenced by the microstructure of the material (grain size), the mean stress of the applied load, the operating temperature and the environment present (Beden *et al*, 2009). Recommendations on ASTM Standard E647-9 establish that crack growth comes to a stop when it is in the order of 10^{-10} m/cycle which implies a crack extension of just 1 mm in 10^7 cycles.

The Paris region was named due to the research work carried out by Paris and Erdogan (1963). In this region the use of Linear Elastic Fracture Mechanics (LEFM) concepts is acceptable due to the fact that experimental data follows a linear relation when using a logarithmic scale, as shown in Figure 2.11. Paris and Erdogan (1963) established a power function (20) to describe the relation between da/dN and ΔK, where C and m are material constants.

$$\frac{da}{dN} = C\ \Delta K^m \tag{20}$$

The previous equation provides a linear relation: $log\left(\frac{da}{dN}\right) = log(C) + m\ log(\Delta K)$ with m as the slope. Nevertheless, it does not account for the R_σ effect on crack growth, neither for the asymptotic behaviour in regions I and II.

In the stable-tearing crack growth region, crack growth rate is high, around 0.01mm/cycle and higher. Crack growth life in these regions is relatively short, which implies that its engineering significance is limited. It seems easy to predict the occurrence of final failure because it should occur when $K_{max} = K_c$. However, K_c (the stress intensity factor that causes final failure) for structural materials is not usually a constant material property (Schijve, 2004).

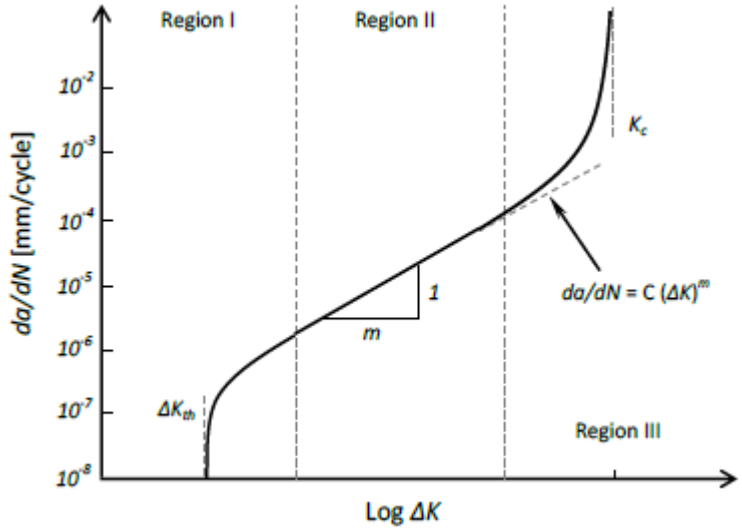

Figure 2.11 – Three regions of the crack growth rate as a function of ΔK (Correia, 2014)

Several alternative proposals for the simple Paris' model are available in literature. These alternatives are more complex fatigue crack propagation relations that intend to overcome Paris' model limitations. In order to take stress ratio effect on fatigue crack growth rate into account, Walker (1970) proposed relation (21). It coincides with Paris relation for $R_\sigma = 0$. In addition to C and m constants, already existing in the Paris' model, it introduces a third fitting parameter, γ.

$$\frac{da}{dN} = C \left[\frac{\Delta K}{(1-R_\sigma)^{1-\gamma}}\right]^m \tag{21}$$

With this equation Walker intended to provide a single straight line regardless of the stress ratio used to obtain data. He reached his goal by introducing the γ parameter which is determined by trial and error. Its value is the one that best represents data along a single straight line on a double logarithmic scale of da/dN versus $\overline{\Delta K}$, with $\overline{\Delta K}$ defined in (22) equation. Nonetheless, it is possible that no value of γ can be found, which means that the Walker equation cannot be used. Another special case occurs when γ is equal to one, which indicates that stress ratio has no effect on data.

$$\overline{\Delta K} = \frac{\Delta K}{(1-R_\sigma)^{1-\gamma}} \tag{22}$$

Both Paris and Walker's models are valid for crack propagation in region II. However, Forman (1972) presented an extension of Walker's model for region III expressed by equation (23). It indicates that as K_{max} approaches K_c, crack growth rate tends to infinity.

$$\frac{da}{dN} = \frac{C\ \Delta K^m}{(1-R_\sigma)(K_c - K_{max})} \tag{23}$$

Furthermore, Hartman and Schijve proposed a general expression which fits the three crack propagation regions given by equation (24). It expresses a sigmoidal shaped curve with vertical asymptotes at $K_{max} = K_c$ and $\Delta K = \Delta K_{th}$. However, stress ratio dependency of ΔK_{th} is not directly contemplated in the relation, which stands as a limitation. Moreover, the correct value of K_c should be used.

$$\frac{da}{dN} = \frac{C\ (\Delta K - \Delta K_{th})^m}{(1-R_\sigma)K_c - \Delta K} \tag{24}$$

The above presented relations belong to LEFM because they make use of linear parameter ΔK. This means that those relations are formulated to be applicable for cracks with limited plasticity ahead of the crack tip. Consequently, several proposals have been made to correlate fatigue crack growth for generalized elastoplastic conditions with Elastoplastic Fracture Mechanics

(EFM) parameters. One example is the case of using the J-Integral instead of ΔK, as proposed by Dowling and Begley (1976) – see equation (25). Even though this equation only fits for region II and does not include stress ratio effect, as the Paris relation, it can be applied in situations of large scale yielding.

$$\frac{da}{dN} = C\ \Delta J^m \tag{25}$$

All the previously presented relations are suitable for constant amplitude loading conditions, since variable amplitude loading conditions may introduce significant changes in the crack growing process like the retardation effect on crack propagation induced by an overload, for example. This fact becomes important since the majority of structures are subjected to variable amplitude loading. Typically, the fatigue crack growth approach for variable amplitude loading is to neglect the sequence of effects, which generally leads to a conservative estimate, sufficient for a preliminary analysis. It is also known that a more detailed analysis, where load sequence effects are considered, will not lead to better practical results (Beden *et al*, 2009).

Being aware of this, Wheeler developed a model with a retardation parameter in the propagation law in order to simulate the effects induced by single overloads. Afterwards, Willenborg improved Wheeler's model so as to also consider underloads. There is a widely used fatigue crack propagation model based on Willenborg's model, called NASGRO model. The designers of NASGRO worked in Willenborg´s model in order to account for the reduction of retardation due to underloads (Correia, 2014).

2.3.4.3 Fatigue modelling based on Fracture Mechanics

The reliability of fatigue life predictions of mechanical components or structural details based on Fracture Mechanics is largely dependent on the availability of accurate fatigue crack propagation laws. Normally, the use of Fracture Mechanics based on fatigue propagation models consists in residual fatigue life assessment of mechanical components or structural details containing initially known defects acting as cracks. Thereby, crack propagation laws should be integrated as indicated by equation (26) where a_i is the initial crack size and a_f the final crack size, which is established by unstable crack propagation, dictated by material toughness, or plastic failure at the net section (Correia, 2014).

$$\frac{da}{dN} = f(\Delta K, R_\sigma \dots) \Rightarrow N_f = \int_{a_i}^{a_f} \frac{da}{f(\Delta K, R_\sigma, \dots)} \tag{26}$$

However, the integration of fatigue crack growth relations can also be used for total fatigue life assessment of components, thus neglecting crack initiation and considering fatigue life as a process of fatigue crack propagation. This approach implies the determination of the initial crack size for crack growth analysis which is not an easy task. This difficulty may be overcome

by using empirical assumed crack length around 0.25 to 1 mm for metals underestimating fatigue life of the component. Some authors proposed a local approach based on strain-life relations to reach the number of cycles to initiate such macro-crack, however, sometimes, a demanding calibration process is needed (Correia, 2014).

A non-destructive inspection (NDI) technique stands as an alternative for initial defect measurement but it is dependent on its detection capacity. It is a conservative assumption to consider an initial defect coinciding with the size of the NDI detection limit. There is a standard practice to establish an equivalent initial flaw size (EIFS) in order to estimate the initial crack size for fatigue life predictions based on Fracture Mechanics. The calculation of EIFS is usually performed using a trial and error back-extrapolation (inverse) methodology. This approach uses fatigue crack growth analysis with an assumed initial crack geometry and size to match the material failure data (stress-life) (Correia, 2014).

Previous research has shown that the obtained EIFS seems to be dependent on stress level when using the back-extrapolation method. This may be considered a problem because EIFS must be applicable to a wide range of stress levels. It should be noted that the EIFS parameter is a quantity extrapolated from experimental data, simply to facilitate fatigue life prediction by using only long crack growth analysis and avoiding difficulties of short crack growth modelling. The use of EIFS concept is not widely spread due to the large amount of test data required to develop a reliable EIFS distribution (Correia, 2014).

2.3.5 Procedure of S-N prediction based on crack initiation and propagation

In order to establish a fatigue model for studying the fatigue life of a structural detail (bolted connection, for example), the contribution of crack initiation and propagation phases should be determined. As discussed in the previous topics, while for fatigue crack initiation, strain-life fatigue relations obtained with small-scale tests of smooth specimens are the best option, for modelling the fatigue crack propagation regime, the integration of LEFM relations must be the chosen technique. As mentioned before, trying to define the transition between crack initiation and crack propagation regimes according to crack dimension is not a consensus subject in literature; nonetheless the majority of authors define the macroscopic size within 0.25-1 mm crack size range (De Jesus *et al*, 2014).

In relation to fatigue crack initiation, the widely used strain-life relation proposed in Morrow (1965), before stated in equation (9) should be used. In order to take the mean stress effect into account, σ_{med} is added, as equation (27) shows (De Jesus *et al*, 2014).

$$\frac{\Delta\varepsilon}{2} = \frac{\Delta\varepsilon^E}{2} + \frac{\Delta\varepsilon^P}{2} = \frac{\sigma'_f - \sigma_{loc,med}}{E}(2N_i)^b + \varepsilon_f(2N_i)^c \quad (27)$$

Local elastoplastic analysis should be performed using the system of equations (28) where the analytical Neuber approach (1961) (first equation) and the cyclic curve of the material expressed by the Ramber-Osgood relation (1943) (second equation) are applied together. This system of equations is used to compute the maximum local stress, σ_{loc}, and strain, ε_{loc}, where K'' and n'' are, respectively, the monotonic strain hardening coefficient and exponent, K_t is the elastic stress concentration factor and σ_{nom} is the nominal stress (De Jesus *et al*, 2014).

$$\begin{cases} \dfrac{\sigma_{loc}^2}{E} + \sigma_{loc}\left(\dfrac{\sigma_{loc}}{K''}\right)^{1/n''} = \dfrac{K_t^2\sigma_{nom}^2}{E} \\ \varepsilon_{loc} = \dfrac{\sigma_{loc}}{E} + \left(\dfrac{\sigma_{loc}}{K''}\right)^{1/n''} \end{cases} \tag{28}$$

Regarding cyclic loading, the previous system of equations should be adjusted replacing the maximum values by range values, as presented in (29). The monotonic strain hardening coefficient and exponent may also be replaced by K' and n' corresponding to the cyclic parameters counterparts (De Jesus *et al*, 2014).

$$\begin{cases} \dfrac{\Delta\sigma_{loc}^2}{E} + 2\Delta\sigma_{loc}\left(\dfrac{\Delta\sigma_{loc}}{2K'}\right)^{1/n'} = \dfrac{K_t^2\Delta\sigma_{nom}^2}{E} \\ \Delta\varepsilon_{loc} = \dfrac{\Delta\sigma_{loc}}{E} + \left(\dfrac{\Delta\sigma_{loc}}{2K'}\right)^{1/n'} \end{cases} \tag{29}$$

The remaining parameter to be defined is mean local stress, $\sigma_{loc,med}$, which can be computed as presented in equation (30).

$$\sigma_{loc,med} = \sigma_{loc} - \frac{\Delta\sigma}{2} \tag{30}$$

Rather than the proposed elastoplastic analysis, a fully elastoplastic finite element analysis could be performed, even though this simplified approach is considerably less time consuming. Nonetheless, the required elastic stress concentration factor needs to be determined using finite element analysis, assuming linear elastic materials. (De Jesus *et al*, 2014).

In regard to modelling fatigue crack propagation using LEFM, the crack propagation law presented in equation (20) proposed by Paris stands as the best option. The following step is to determine the number of cycles to failure integrating the Paris relation between the crack initial size, a_i, and the final size, a_f, as previously expressed by equation (26). As mentioned before, the definition of the crack initial size is a controversial issue, however it has a significant influence in the number of cycles to propagate the crack since stress intensity factor range assumes smaller values in the first stages of crack propagation. In relation to the final crack size, it can have the same value of the net section of the connection or it can be defined with a value for which the maximum stress intensity factor reaches its critical value (Jesus *et al*, 2014).

In order to perform the integration of Paris equation, stress intensity factor range should be a function of crack length, a. An approximate procedure of small increments in crack length, Δa, should be established, in which stress intensity factor is assumed as constant and equal to its value at the beginning of the increments, resulting in increments in the number of cycles to failure, as equation (31) expresses. (De Jesus *et al*, 2014).

$$\Delta N = \frac{1}{C}\frac{1}{\Delta K^m}\Delta a \tag{31}$$

2.3.6 Procedure of S-N prediction based on local unified model

This topic will deal with a probabilistic approach to generate S-N curves for distinct stress ratios (p-S-N_f-R_σ) for both fatigue crack initiation (p-S-N_i-R_σ) and crack propagation periods (p-S-N_P-R_σ), using local models based on probabilistic ε-N or Smith-Watson-Topper (SWT)-N fields. This procedure was developed considering the UniGrow model, thus its simplified overview is presented below (Correia *et al*, 2013).

The UniGrow model was proposed in Noroozi *et al* (2005) and it has been classed as a residual stress based crack propagation model. It considers a material discretization using discrete elementary blocks defined by the finite dimension ρ^*, as shown in Figure 2.12 (a). In addition, the fatigue crack tip is established to be equivalent to a notch with radius equal to ρ^*, as illustrated in Figure 2.12 (b). The fatigue crack growth process, ruled by fatigue crack growth rate expressed in equation (32), is assumed to be composed of successive crack increments due to crack re-initiations over distance ρ^*. In equation (32), N_f represents the number of cycles required for the material representative element to fail.

$$\frac{da}{dN} = \frac{\rho^*}{N_f} \tag{32}$$

While parameter N_f can be determined by making use of strain-life relations, namely the SWT damage parameter (11) or Morrow's equation (9), the required material representative element size, ρ^*, is assessed using fatigue crack propagation data obtained with compact tension specimens (CT specimens).

Therefore, a general procedure to generate p-S-N-R_σ fields for notch details can be presented as follows (Correia *et al*, 2013):
- rather than using deterministic SWT-N or ε-N models, estimation of probabilistic parameters using experimental fatigue data from smooth specimens should be used in order to establish probabilistic fatigue models (p-SWT-N or p-ε-N fields). These probabilistic fields will serve as base for both crack initiation and propagation phases;

- using a trial and error procedure, the elementary material block size, ρ^*, must be estimated in order to establish a good approximation between fatigue crack propagation prediction and experimental crack propagation data, for distinct stress ratios;
- an elastoplastic finite element analysis of the structural notch detail should be the following step. The aim is to evaluate the local stresses/strains at the first element block size ahead of the notch root;
- make use of the p-SWT-N or p-ε-N models to obtain the probabilistic representation of S-N curves for crack initiation period in the structural detail (p-S-N_i-R_σ fields);
- use the previously computed elementary material block size, and adapt the UniGrow model in order to enable the use of probabilistic fatigue models p-SWT-N or p-ε-N and evaluate fatigue crack propagation in the structural detail (p-S-N_P-R_σ fields);
- finally, proceed to the combination of fatigue crack initiation and crack propagation p-S-N fields using equation (1) resulting in global S-N curves, p-S-N_f-R_σ.

The proposed procedure to derive probabilistic S-N curves for structural details was used by Correia *et al* (2013) in a notched rectangular plate made of pressure vessel steel and it proved to be quite efficient. Both fatigue crack initiation and crack propagation prediction showed satisfactory results.

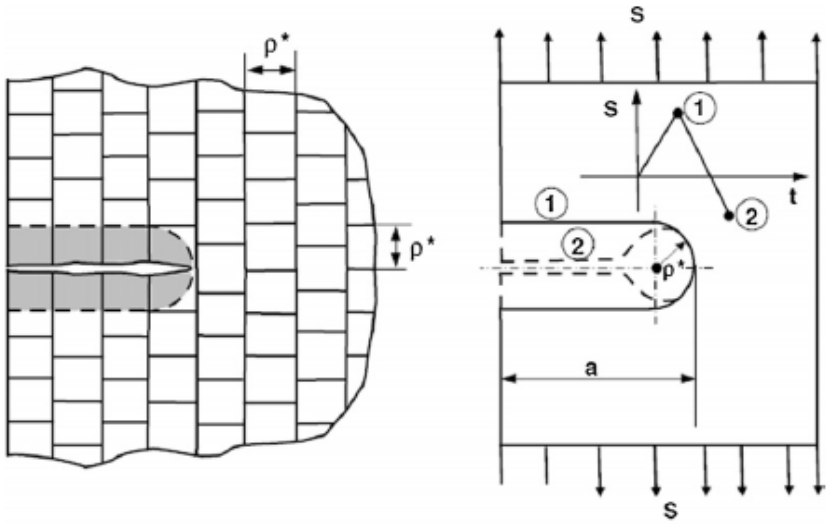

(a) (b)

Figure 2.12: (a) Crack and discrete elementary blocks; (b) Crack shape at the tensile maximum and compressive minimum loads (Correia *et al*, 2013)

2.3.7 Procedure of S-N prediction based on an equivalent initial flaw size model

Fatigue life predictions based on Fracture Mechanics approaches can also be performed using the equivalent initial flaw size (EIFS) concept. This concept assumes that materials have intrinsic defects that act as initial cracks. The use of these small cracks implies that the applicability of LEFM must not be appropriate, thus the use of EFM parameters, to correlate

fatigue crack growth, is proposed by some authors. Therefore, the J-Integral concept, previously presented in equation (25), stands as a good option. The material behaviour based on the cyclic stress-strain curve described by the Ramberg-Osgood relation (10) should be used to calculate the ΔJ value (Correia *et al*, 2016).

Alves *et a*l (2015) proposed an extension of equation (25) in order to have in account fatigue crack propagation regime I introducing a threshold value of the cyclic J-Integral, ΔJ_{th}, as equation (33) shows.

$$\frac{da}{dN} = C(\Delta J - \Delta J_{th})^m \text{ for } \Delta J \geq \Delta J_{th} \quad (33)$$

A recent model proposed by Castillo and Fernández-Canteli (CCS) (2014) for fatigue crack propagation should be considered. It is based on the assumption that crack growth follows a cumulative distribution function. Making use of an appropriate dimensional analysis leading to normalized non-dimensional parameters, the inconvenience of using dimensional parameters (ΔK, N or a parameters used in the Paris equation, for example) is overcome. However, Correia *et al* (2016) suggest the extension of CCS model to cover the cases of elastoplastic loading, replacing stress intensity factors by cyclic J-Integral counterparts. Finally, the number of cycles to failure of a structural detail can be obtained through a numerical integration of the modified CCS crack growth model between the initial crack size (a_i=EIFS) and the final crack size, a_f (Correia *et al*, 2016).

Consequently, a general procedure is presented to predict S-N curves based on EIFS models:
- the modified CCS crack growth model, along with the cyclic J-Integral, is used to obtain material constants under estimation from fatigue crack propagation data;
- use finite element method in order to perform an elastoplastic stress analysis for the cracked geometry of the structural detail under investigation. The Ramberg-Osgood model should be used to model the elastoplastic behaviour of the material. As such, cyclic J-Integral results can be acquired;
- perform a numerical integration of the modified CCS crack growth equation;
- make use of fatigue S-N data on the structural detail, an estimation of the equivalent initial flaw size parameter should be done;
- finalize with fatigue life prediction for the structural component or mechanical detail.

Correia *et al* (2016) described the use of this general procedure on a double notched plate made of pressure vessel steel. S-N predictions showed satisfactory agreement with experimental data.

3 EXPERIMENTAL APPROACH

3.1 Introduction

Several strategies can be implemented in repairing and strengthening operations of old riveted steel bridges, such as riveting, welding, using HSFG bolts, fitted bolts or resin injected bolts. In this chapter, the concept of injected bolts as well as their advantages when used in structural reinforcement of old and new steel structures is presented. The structural behavior of adhesives used in this type of connections (in most cases epoxy resins) is also addressed.

There are not many studies about fatigue behaviour of bolted connections in which a structural adhesive is used. The main works were carried out by Albrecht *et al* (1984) and more recently by De Jesus *et al* (2010). Experimental results obtained in these two researches are presented in the form of S-N curves. A design curve is proposed for the studied connections through a statistical analysis of obtained results, following the recommendations of ASTM E739-91 Standard. Furthermore, the behaviour of RIBJ with pultruded FRP material under fatigue loading is also studied in this chapter with reference to the research work performed by Zarafi *et al* (2016).

3.2 Resin injected bolted connections – concept and applications

3.2.1 Injection bolts configuration

Injection bolts can be produced from standard bolts adapting them for the resin injection process as mentioned in Annex K of EN 1090-2:2008. As shown in Figure 3.1 (a), connections with injection bolts are characterized by filling the gap between the plates and the bolt with a structural resin. The filling process is usually carried out through an injection hole in the bolt's head. Regarding washer preparation, a groove should be machined in the bottom washer (under the nut) in order to enable the air to escape while the top washer (under the bolt's head) must be prepared to ensure a smooth passage and uniform resin distribution – see Figure 3.1 (b).

After resin develops its finest mechanical properties at the end of the curing process (which can take around seven days according to the product data sheet of some structural adhesives, such as SIKADUR®-30, for example), it is intended to obtain a slip resistant connection. Environmental temperature during injection should be a concern because it influences two important parameters of the resin: the viscosity level and the curing time. Concerning the viscosity level of the resin, it should have such a magnitude which eases the injection process even for small clearances. Manufacturer's indications must be followed in order to obtain the optimum injection temperature. It is also important that the workability time of the resin

(potlife) will be such that allows its injection. In Annex K of EN 1090-2:2008 a potlife of at least 15 minutes is recommended.

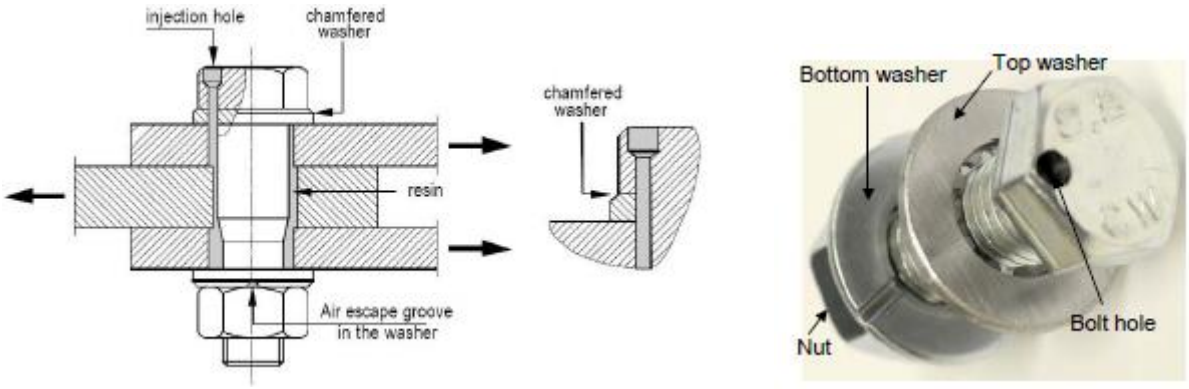

(a) (b)

Figure 3.1 - (a) Injection bolt configuration (Nikolovski, 2009); (b) Adapted bolt and washers (Qureshi and Mottram, 2012)

3.2.2 Applications

Repairing and strengthening operations in old riveted construction have been implemented using injection bolts. *ECCS Publication no. 79* states: "Since 1970 it has been standard practice in The Netherlands to repair old railway bridges and road bridges in this way. […] No failures with injection bolts have been reported.". This document presents a specific case of a riveted bridge in Rotterdam where injection bolts were used to replace faulty rivets. However, this solution can be considered for new constructions, too. Such was the case in the new football stadium for AJAX Amsterdam, where injection bolts were used in the steel structure of the movable roof. This solution ensures that no slip will occur (Gresnigt and Stark, 1996).

In Germany, the first application of injection bolts to repair steel bridges is described in Gresnigt *et al* (2000). Due to the advanced corrosion state of several structural elements, it was decided to apply injection bolts to connect new plates at the corroded areas of the webs of the main girders, as shown in Figure 3.2. The paper mentioned before also describes the long duration creep tests in RIBJ requested by German authorities. Results showed that this solution stands as a good alternative when no slip is allowed.

In Portugal, the first known application of injection bolts was in the steel structure of the bridge originally designed by Edgar Cardoso, in Figueira da Foz, over the Mondego River, in 1980. Although this solution was not stated in the tender documents, the construction company performed a series of monotonic tests in order to prove the good behaviour of such connections in serviceability state and thus justify its application (Mattes, 2007).

Figure 3.2 – Strengthening operations of the web in the main girder using injection bolts (Gresnigt *et al* 2000)

Different strategies can be implemented in the repairing of old riveted steel bridges. Generally, these old structures present advanced corrosion damage, therefore, due to the poor weldability properties of old steel, repairing with welding strengthening plates is not considered. Riveting is no longer a common practice, hence finding good equipment and professionals is a difficult task. This option fell into disuse because riveting is a dangerous (rivets have to be heated) and time-consuming process. Another disadvantage of using rivets is the limited clamping stress that can be created (the positive effect of pretension in such joints will be shown further in this document). The design bearing resistance of the joint is usually quite sufficient to replace faulty rivets (Gresnigt *et al*, 2000).

Another possibility that is excluded is HSFG bolts because it requires a good friction coefficient between contact surfaces. Slip can be avoided with no special treatment on the contact surfaces when using non-preloaded injection bolts, while for HSFG bolts, good friction behaviour has to be secured in order to obtain a satisfactory slip factor (ECCS Publication no. 79, 1994).

After injection and curing of the resin, injection bolts have a structural behaviour similar to fitted bolts in what concerns their slip resistance. However, the use of fitted bolts implies an expensive preparation of the holes (ECCS Publication no. 79, 1994).

Due to the fact that the static design resistance of a preloaded injection bolt is obtained by adding the bearing resistance of the resin to the slip resistance, when the desired load transfer per bolt is high (e.g. lack of available space for bolts in small connections), preloaded injection bolts offer a more compact connection (fewer bolts) when compared to HSFG bolts. Another advantage of implementing injection bolts in a structure is the protection against internal corrosion when the resin is used (ECCS Publication no. 79, 1994).

Nevertheless, there are some disadvantages when injection bolts are used. As mentioned before, bolts and washers have to be adapted to enable the injection process which increases the cost of bolts and washers themselves. Another disadvantage is the additional time spent in preparing the resin and its injection in the cavity. Weather conditions may also be a concern because holes

must be dry during the injection. Using injection bolts can also create some difficulties if the dismantling process is required (ECCS Publication no. 79, 1994).

Material costs for RIBJ are related to the purchase of the bolts themselves (duly adapted for the injection process) and the structural resin. Injection equipment is cheap and although resin is an expensive material, the amount required per bolt is reduced. Bearing in mind that RIBJ the number of bolts can be reduced, final costs can be lower than in other solutions mentioned. The execution of this type of connection depends on the number of bolts, its accessibility and cleaning of the hole. The labour time for injection varies roughly between one and two minutes per bolt (Gresnigt *et al*, 2000).

3.2.3 Structural adhesives

Adhesive is the substance used for holding at least two surfaces in a strong and permanent manner. They are generally used for: attaching surfaces through adhesion; improving strength capacity; contributing to distribute and to transfer the load over a large area. Adhesives can be classified as structural adhesives or non-structural adhesives. In the first situation, the adhesive takes part in the assembly strength and its mechanical properties are important. Non-structural adhesives present lower strength and performance and are normally used for temporary fastening or bonding weak substrates (Miravalles, 2007). This study is restricted to structural adhesives.

As demonstrated in Figure 3.3, there are two failure modes when a structural adhesive is implemented: adhesive failure and cohesive failure. The first occurs when the adhesive and the adherend detaches each other through contact surface, while cohesive failure happens if the failure surface is within the adhesive material (Miravalles, 2007).

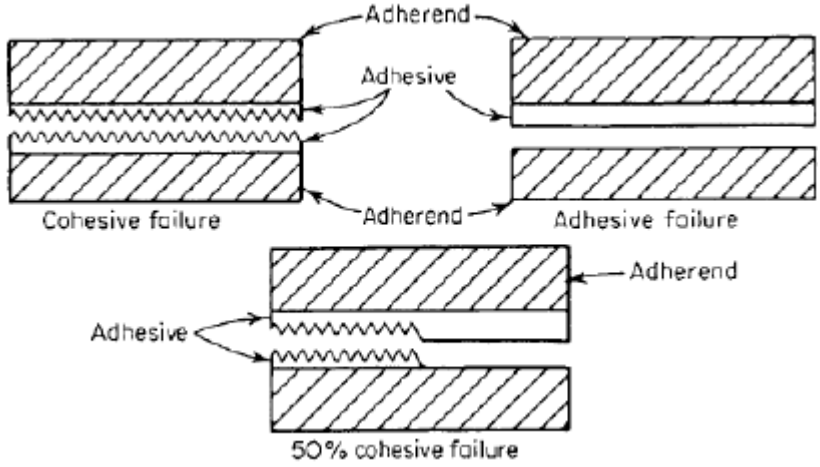

Figure 3.3 – Cohesive and adhesive failure modes (Miravalles, 2007)

Before using adhesives as a material for all applications, the advantages and disadvantages have to be considered. The main benefits of implementing adhesives are: simple process of

application; huge versatility in the materials which it can be applied to; good corrosion resistance. Whilst the main disadvantages are: the need for plain and clean surfaces; they do not develop their strength properties immediately after application (Miravalles, 2007).

When a structural adhesive is used in bolted connections, it is expected that its structural behaviour allows the reduction of stress concentration around the holes or, in other words, it should contribute to distribute and to transfer the load over a large area. Several experimental studies performed in RIBJ have made use of epoxy resins (Sikadur®-30 and RenGel® SW404), since they can provide a cold curing, a suitable viscosity for injection and acceptable mechanical properties (Zarafi *et al*, 2016 and De Jesus *et al*, 2010).

As for the static behaviour of RIBJ, it is known that the bearing resistance of the resin, $f_{b,resin}$, introduces a resistance increase, (ECCS Publication no. 79, 1994). However, for cyclic fatigue loading conditions it is important to study the cyclic elastoplastic behaviour of structural adhesives. Technical information given in the supplier's datasheet is always related to the static performance of structural adhesives and the cyclic properties are never mentioned (Sika@, 2012). Table 3.1 presents the static mechanical strength properties for different types of requests as a function of the curing time, indicated from the manufacturer. It also refers that the Young modulus of the adhesive is equal to 11,2 GPa in tension loading and equal to 9,6 GPa in compression loading.

Cure time	Compressive Strength (+10ºC)	Shear Strength (+15ºC)	Tensile Strength (+15ºC)
1 day	50-60 MPa	3-5 MPa	18-21 MPa
3 days	65-75 MPa	13-16 MPa	21-24 MPa
7 days	70-80 MPa	14-17 MPa	24-27 MPa
14 days	-	15-18 MPa	25-28 MPa

Table 3.1 – Sikadur®-30 strength properties evolution with cure time (Sika@, 2012)

More recently, a new epoxy based resin was introduced in the market, with a commercial name Sikadur®-52, and it is characterized by its high strength properties, as shown in Table 3.2.

Cure time	Compressive Strength (+23ºC)	Shear Strength (+23ºC)	Tensile Strength (+23ºC)
7 days	Aprox. 52 MPa	Aprox. 61 MPa	Aprox. 37 MPa

Table 3.2 - Sikadur®-52 strength properties (Sika@, 2016)

Future investigations should be made in order to characterize the fatigue properties of these structural adhesives.

3.3 Analysis of experimental campaigns performed in joints with adhesives

3.3.1 Steel-steel connections

3.3.1.1 Statistical Analysis

As mentioned before, fatigue experimental data are usually plotted on graphs relating applied stresses with the number of cycles to failure, *i.e.*, S-N curves. Since test specimens and loading conditions are never completely equal, scatter on the results is unavoidable. However, statistical methods can be used to overcome this matter and establish practical solutions to analyse the obtained data. A statistical method to assist in the analysis of fatigue test data is stated in ASTM standard E739-91:1998, which was the chosen methodology to perform the following statistical treatments.

For the following case studies, mean S-N curves were defined adapting a linear model to the results given by the following equation (34). One way to perform this arrangement is rewriting Basquin equation (2), as equation (35) shows. Then, the dependent variable, Y, is defined as $Y = \log \Delta\sigma$, the independent variable, X, as $X = \log N_f$, the parameter A as $A = 1/m \cdot \log C$, and B as $B = -1/m$.

$$Y = A + B \cdot X \tag{34}$$

$$\log \Delta\sigma = \frac{1}{m} \cdot \log C - \frac{1}{m} \cdot \log N_f \tag{35}$$

For the estimation of A and B parameters, equations (36) and (37) should be used, where $\overline{Y}$ and $\overline{X}$ are the mean values of the experimental data $X_j = \log N_{f,j}$ and $Y_j = \log \Delta\sigma_j$, respectively and *k* is the number of tested specimens.

$$A = \overline{Y} - \mathrm{B} \cdot \overline{X} \tag{36}$$

$$B = \frac{\sum_{j=1}^{k}(X_j - \overline{X})(Y_j - \overline{Y})}{\sum_{j=1}^{k}(X_j - \overline{X})^2} \tag{37}$$

Since rectilinear confident bands are usually implemented in fatigue design codes (EC3-1-9 for example), they were defined for the obtained S-N curves as equation (38) shows, where α is an integer number (in this analysis it is assumed that $\alpha = 1$ and 2) and *S* is the standard deviation of the residuals calculated from equation (39). If α assumes value 1, the confidence band will cover approximately 68% of the obtained data, whereas if α is equal to 2, the covered values will rise to around 95%. Consequently, fatigue design curves were chosen for $\alpha = -2$.

$$Y = A + B \cdot X \pm \alpha \cdot S \tag{38}$$

$$S^2 = \frac{\sum_{j=1}^{k}(Y_j - A - B \cdot X_j)^2}{k-2} \tag{39}$$

3.3.1.2 Case study: De Jesus *et al* (2010)

In De Jesus *et al* (2010), fatigue tests were conducted with standard bolted connections and RIBJ produced with material from Portuguese old bridges. Furthermore, two different geometries were used: double shear connection made of puddle iron from the Fão Bridge and single shear connection made of construction steel (similar to current steels) extracted from the Trezoi Bridge. Specimens scheme of the studied connections is presented in Figure 3.4. A torque of 80 N.m was applied in bolts of all specimens. Bolts, nuts and washers were adapted to allow resin injection in order to fill in the radial clearance of 1 mm between bolts and plates.

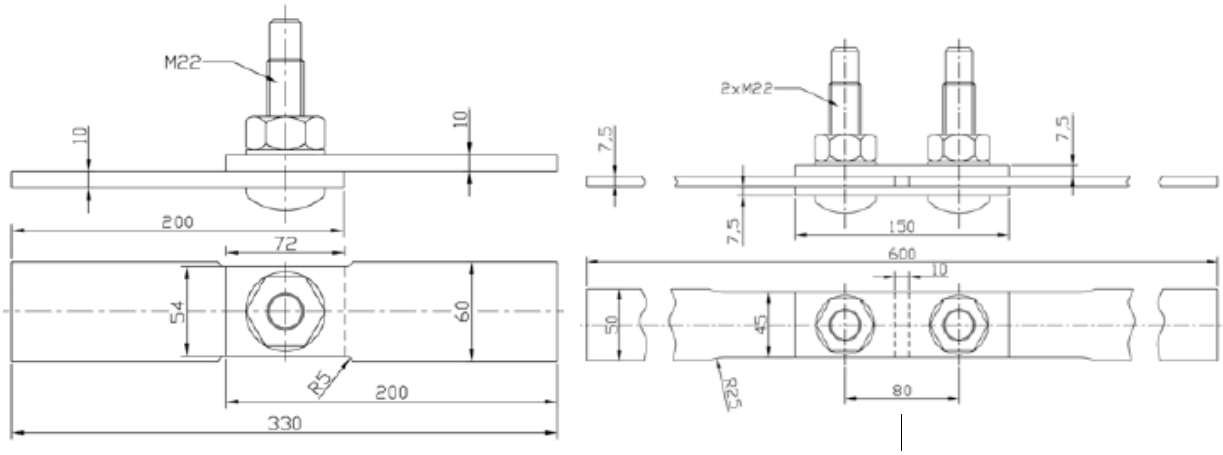

(a) (b)

Figure 3.4: (a) Single shear connection geometry; (b) Double shear connection geometry (Jesus *et al*, 2010)

The previously presented epoxy-based resin, Sikadur®-30, was used in all resin-injected bolts and a curing time of at least eight days was implemented. Figure 3.5 (a) and (b) presents the fatigue data from the experimental tests performed in single and double shear connections, respectively. One test for standard bolts was a run-out and it is identified in the figure with an arrow.

Fatigue results from single and double shear connections were plotted in order to obtain mean S-N curves, as shown in Figure 3.6 and Figure 3.7, respectively. Since for double shear connections made of resin injected bolts only one stress range level was tested, no mean S-N curve is described.

For both single and double shear connections, the use of resin injected bolts led to lower fatigue strength results. A possible explanation to this observation is advanced in the paper and it is

related to the effects of preload. Clamping stress has a beneficial effect on bolted connection due to the reduction of stress concentration around the holes. In standard bolts, compressive contact stresses between the bolt and the hole increase the thickness of plates, due to the Poisson effect, which leads to an increase of clamping stress. On the other hand, filling the clearance in the hole with injected resin produces a redistribution of stresses around the hole which leads to a reduction in the magnitude of compressive stresses, and the clamping stresses, as a consequence. However, this assumption requests further investigation, namely more testing and numerical simulations.

	Δσ (MPa)	Nf (cycles)
Resin-injected bolts	355,5	376856
	355,5	102854
	355,5	166294
	355,5	52949
	355,5	1321738
	355,5	183212
	355,5	130935
Standard bolts	355,5	3245417 →
	377	428551
	377	556452
	398,6	72355
	398,5	666412
	398,5	417582
	355,5	1544535

(a)

	Δσ (MPa)	Nf (cycles)
Resin-injected bolts	361,8	91993
	362,6	120808
	271,5	325865
	271,9	235780
Standard bolts	362,2	297700
	271,3	827824
	271,4	765606

(b)

Figure 3.5 - Fatigue experimental data: (a) Single shear connections; (b) double shear connections (Jesus *et al*, 2010)

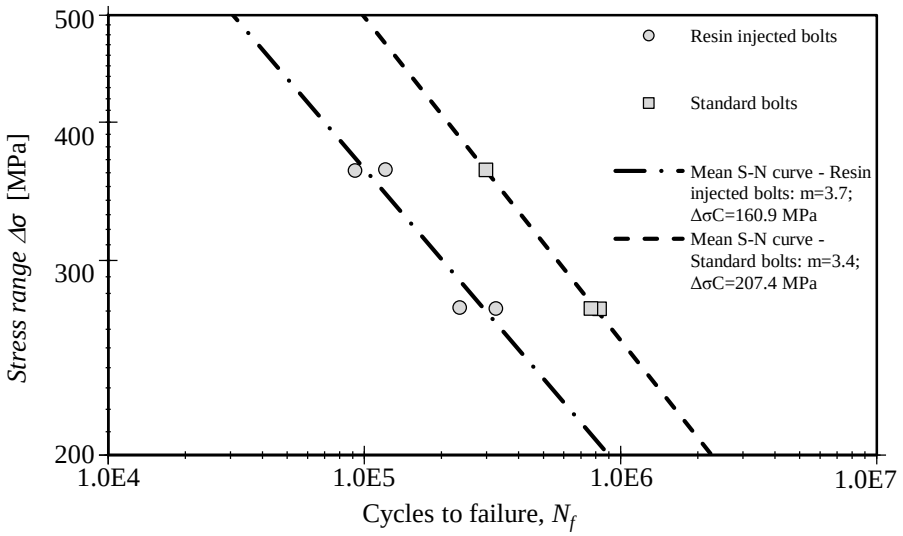

Figure 3.6 – Fatigue experimental results for single shear connections – Trezói Bridge

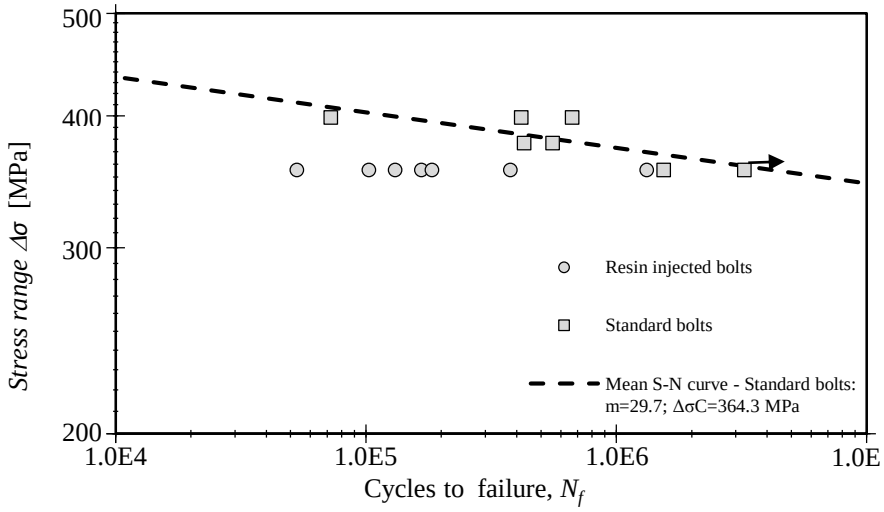

Figure 3.7 – Fatigue experimental results for double shear connections – Fão Bridge

Despite the evidence of fatigue strength reduction, when resin-injected bolts are used, these tests are characterized for their small number of samples along with a significant scatter on the obtained results. For example, double shear connections with resin injected bolts presented differences of nearly one million endured cycles for the same stress range.

Fatigue experimental data of the previous tests were subjected to a statistical analysis as stated in the previous subchapter. It should be noted that, to perform a reliable estimation of the fatigue strength of a structural detail in high or low cycle fatigue, experimental campaigns should consider a reasonable diversity of tested stress ranges (usually four different values). In the two cases presented before, few stress ranges were tested, along with a small number of specimens. However, since there are no more data available in literature for similar tests, the statistical analysis for estimation of a design curve was implemented. Components of statistical treatment performed with experimental results for single shear connections is presented in Figure 3.8.

Figures 3.9 and 3.10 show the confident bands of ±S (68%) and ±2S (95%) for both single and double connections, respectively. Since the number of tested specimens is reduced and the use of resin-injected bolts produced a consistent reduction of fatigue strength, these confident bands were obtained for all tested specimens (with and without resin-injection).

Consequently, through the statistical treatment performed with experimental results for single shear connections in the 95% confident band, the lower boundary is given by a fatigue curve defined by m=7.4 and $\Delta\sigma_C$=187.9 MPa. Experimental results for double shear connections do not cover a sufficient variety of stress ranges, thus the obtained mean S-N curve is meaningless. Therefore, in this case the design curve was defined taking into account the same slope obtained for single shear connections (m=7.4) and with a detail category, $\Delta\sigma_C$, so that all data points are covered ($\Delta\sigma_C$=188.3 MPa).

Variable	Meaning	Value
k	Number of tested specimens	7
$\overline{X}$	Mean value of the independent variable	5,46
$\overline{Y}$	Mean value of the dependent variable	2,49
A	Y intersect of the regression line	3,23
B	Slope of the regression line	-0,14
S^2	Variance	0,002
S	Standard deviation	0,05
R	Coefficient of correlation	-0,74
R^2	Coeficient of determination	0,54

Table 3.8 – Components of statistical treatment performed with experimental results for single shear connections.

The S-N curves proposed in EC3-1-9 are also included in the graphs. This standard does not distinguish the fatigue behaviour of connections with resin injected bolts and standard bolts since the same detailed category is suggested for both. For single shear connections, EC3-1-9 recommends class 90 when preloaded bolts are included and class 80 for connections with non-preload bolts. In the case of double shear connections, this standard indicates class 112 when preloaded bolts are included and class 90 for connections with non-preloaded bolts. Analysing both graphs, the Eurocode S-N curves are generally conservative, since only one data point (referred to single shear connections built with resin injected bolts) stands below the EC3-1-9 curve.

For both single and double shear connections, design curves have smaller slope when compared to the Eurocode S-N curves. Consequently, for high-cycle fatigue these code curve may present conservative results.

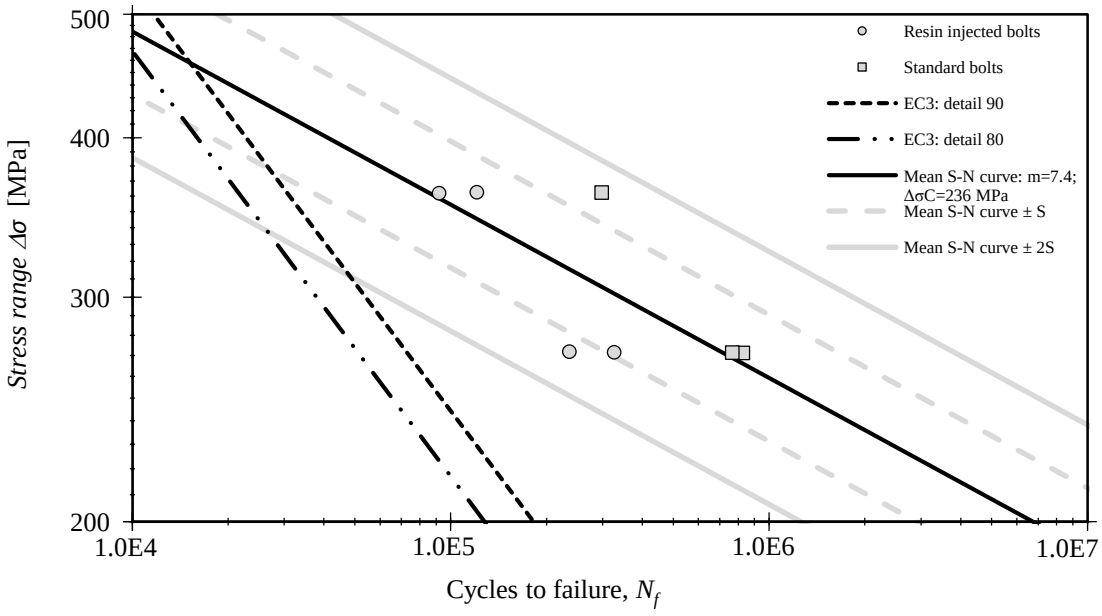

Figure 3.9 – Statistical analysis of fatigue experimental data: single shear connections

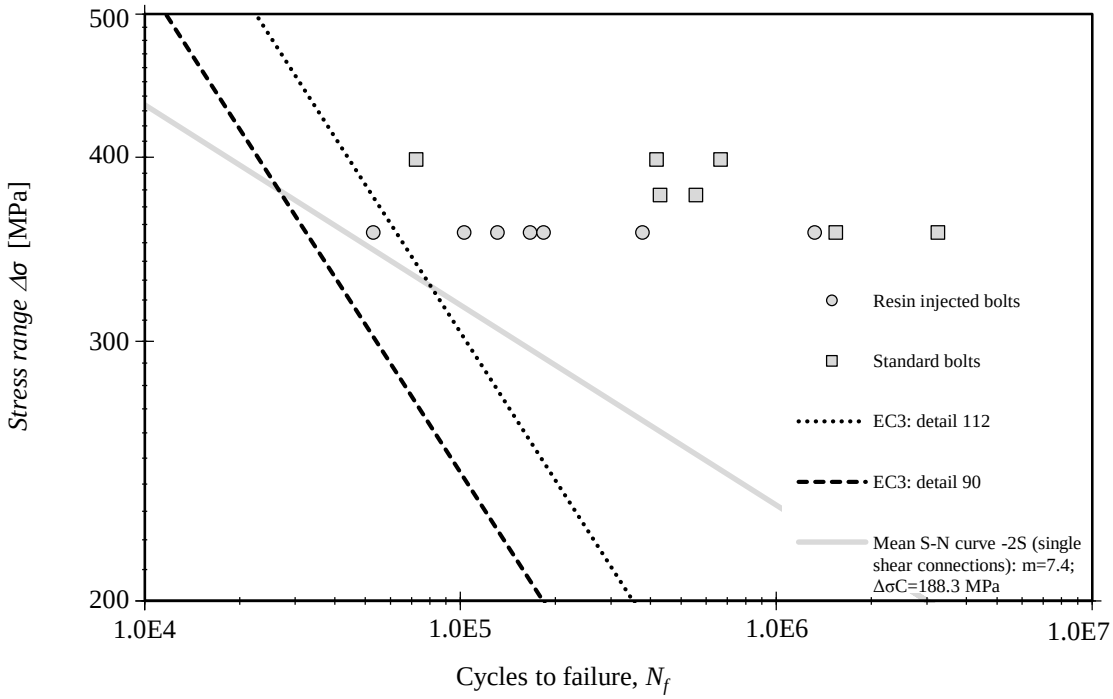

Figure 3.10 – Statistical analysis of fatigue experimental data: double shear connections

3.3.1.3 Case study: Albrecht *et al* (1984)

Concerning the fatigue experimental campaign performed by Albrecht *et al* (1984), an adhesive material is applied on the plate surfaces in order to prolong fatigue life and increase the static strength of bolted joints. It is expected that the adhesive will help to distribute and to transfer the load over a large area, thus reducing stress concentrations. Consequently, this structural solution might be implemented instead of welded details with low fatigue strength, for example.

Two different types of specimens were used. The differences are in the number of bolts and in the geometry of the plates. A scheme of the tested specimens is presented in Figure 3.11.

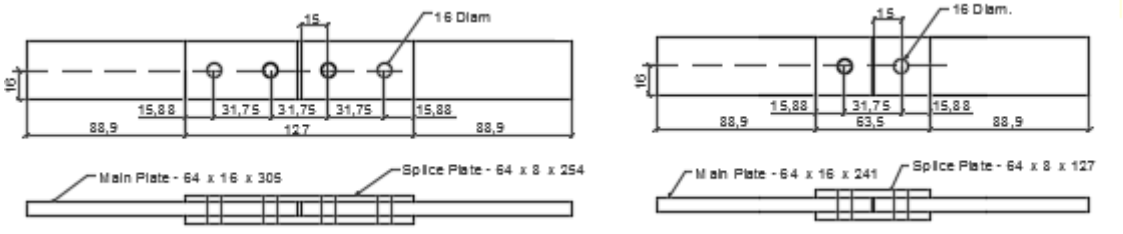

Figure 3.11 – Geometry of the tested specimens: a) Two-bolt specimens; b) One-bolt specimens (dimensions in mm) (adapted from Albrecht *et al* 1984)

Steel plates were produced under the indications of ASTM A588 Standard Specification for High-Strength Low-Alloy Structural Steel. High-strength bolts with 16 mm diameter were used,

as well as hardened steel washers and hex nuts. Bolts were tensioned with 84,5 kN. The adhesive chosen to perform the experimental campaign was Versilok 201, an acrylic adhesive. Through previous comparative researches with several structural adhesives, Versilok 201 has shown higher shear and tensile strength along with a small curing time (Albrecht *et al*, 1984). Specimens with the adhesive applied on its contact surfaces are called bonded specimens while specimens with no adhesive are non-bonded specimens.

Tests were conducted under a sinusoidal cyclic load wave with constant amplitude, and different frequencies were tested (4, 6, 8 and 10 Hz). Figure 3.12 summarizes the fatigue data from two and one bolt specimens.

	Δσ (MPa)	Nf (cycles)
Bonded	219	2001000
	219	1790000
	219	10003000 →
	219	3170000
	285	683000
	285	733000
	285	793000
	285	911000
Non-Bonded	171	2678000 →
	171	9412000 →
	200	10050000 →
	200	10024000 →
	219	678000
	219	2509000
	219	6538000
	219	1170000
	285	612000
	285	244000
	285	494000
	285	535000

(a)

	Δσ (MPa)	Nf (cycles)
Bonded	219	2001000
	219	1790000
	219	10003000 →
	219	3170000
	285	683000
	285	733000
	285	793000
	285	911000
Non-Bonded	171	2678000 →
	171	9412000 →
	200	10050000 →
	200	10024000 →
	219	678000
	219	2509000
	219	6538000
	219	1170000
	285	612000
	285	244000
	285	494000
	285	535000

(b)

Figure 3.12 – Fatigue experimental data: (a) Two-bolt specimens; (b) One-bolt specimens (Albrecht *et al*, 1984)

Fatigue results from two-bolt and one-bolt specimens were plotted in order to obtain mean S-N curves, as shown in Figure 3.13 and Figure 3.14, respectively. Despite some scatter in results for two-bolt specimens, it can be observed that the mean S-N curve for bonded specimens presents better results when compared to the mean S-N curve for non-bonded specimens. The results obtained for one-bolt specimens have a significant low quality (huge scatter). Meaningless values were obtained due to run-outs or early rupture. In this case, there is no clear

beneficial effect of using bonded specimens since mean S-N curves for bonded and non-bonded specimens are similar, and for low-cycle fatigue the use of bonded specimens led to consistent fatigue strength reduction.

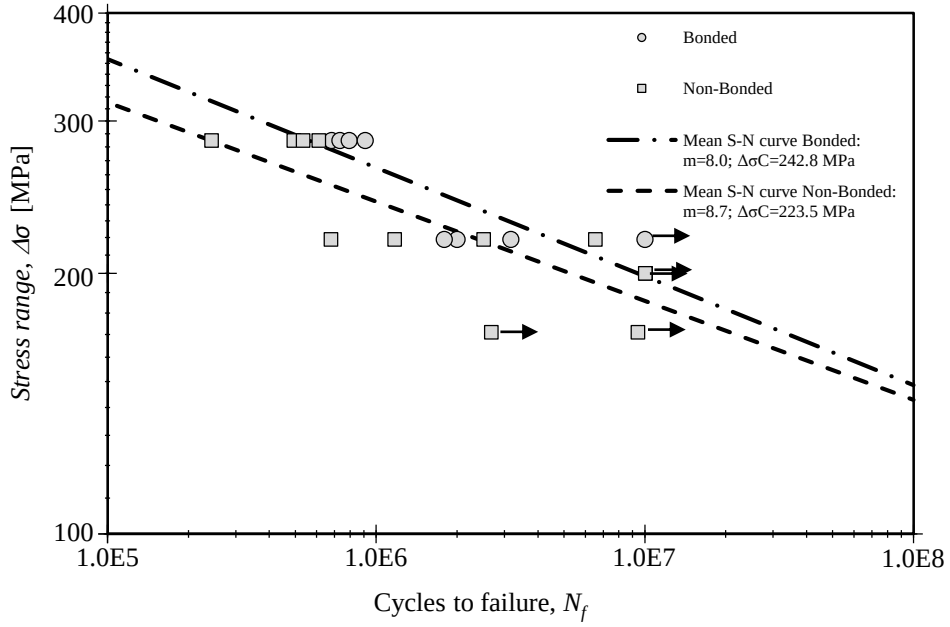

Figure 3.13 – Fatigue test data for two-bolt specimens

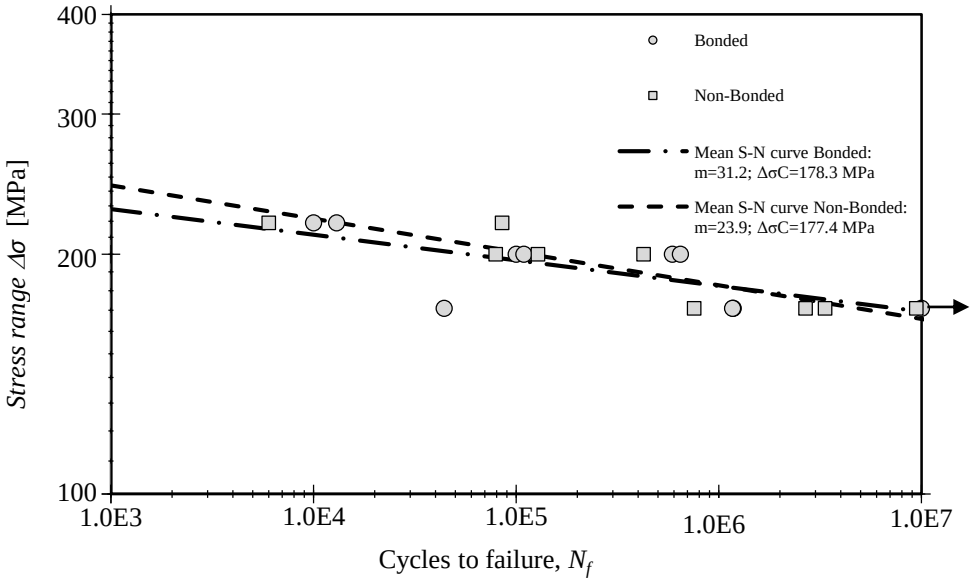

Figure 3.14 - Fatigue test data for one-bolt specimens

Components of statistical treatment performed with experimental results for two-bolt specimens is presented in Figure 3.15. Furthermore, Figures 3.16 and 3.17 show confident bands of ±S (68%) and ±2S (95%) for two-bolt and one-bolt specimens, respectively. As in the case of De Jesus *et al* 2010, there is no sufficient variety in the tested stress ranges, especially for bonded specimens. Therefore, confident bands were obtained for all tested specimens (bonded and non-bonded specimens).

Although EC3-1-9 does not specify a detail category for bonded connections, fatigue strength curves with detail category 112 and 90 might be appropriate. Thus, they were also included in the graphs. For two-bolt specimens, fatigue experimental data presents good results since all points are above EC3 curves, however, when the number of bolts is reduced, fatigue strength decreases dramatically and EC3 curves are no longer conservative.

Consequently, through the statistical treatment performed with experimental results for two-bolt specimens, for the 95% confident band, the lower boundary is given by a fatigue curve defined by m=8.4 and $\Delta\sigma_C$=188.6 MPa. Due to the low quality of the results obtained for one-bolt specimens, the design curve was defined taking into account the same slope obtained for two-bolt specimens (m=8.4) and with a detail category, $\Delta\sigma_C$, so that all data points are covered ($\Delta\sigma_C$=102.5 MPa).

Variable	Meaning	Value
k	Number of tested specimens	20
$\overline{X}$	Mean value of the independent variable	6,24
$\overline{Y}$	Mean value of the dependent variable	2,37
A	Y intersect of the regression line	3,12
B	Slope of the regression line	-0,12
S^2	Variance	0,002
S	Standard deviation	0,04
R	Coefficient of correlation	-0,79
R^2	Coeficient of determination	0,63

Table 3.15 - Components of the statistical treatment performed with experimental results for two-bolt specimens

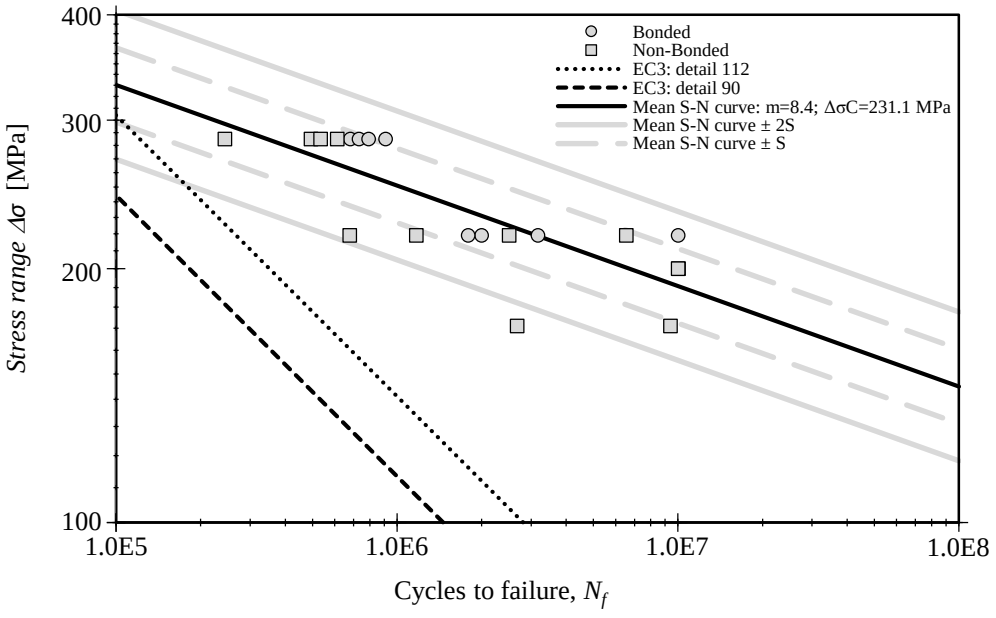

Figure 3.16 - Statistical analysis of fatigue experimental data: two-bolt specimens

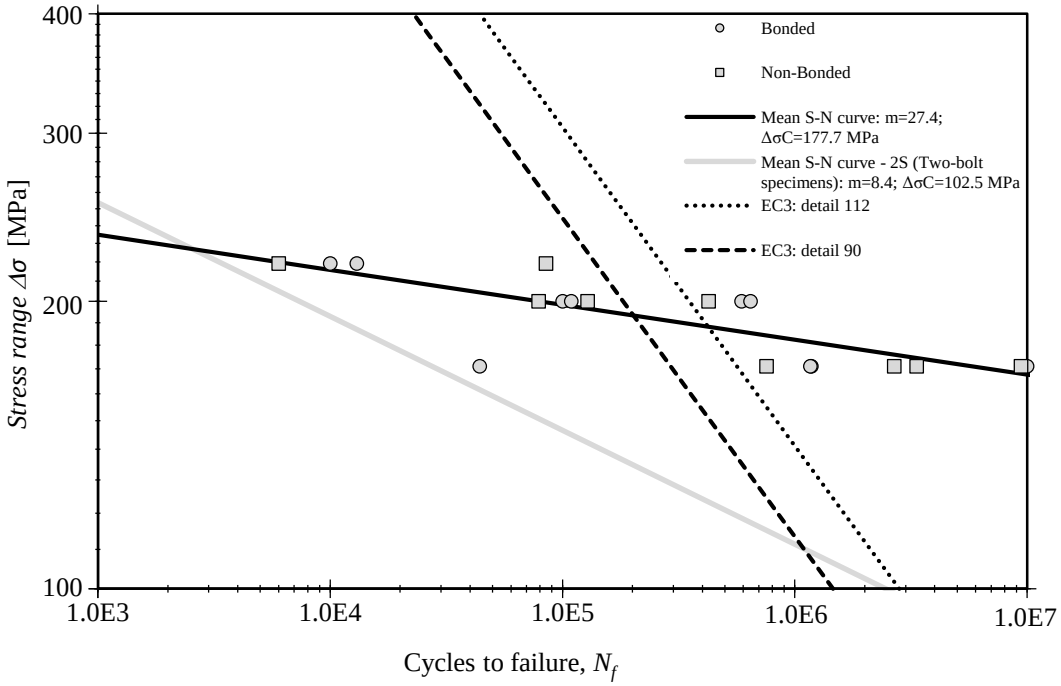

Figure 3.17 - Statistical analysis of fatigue experimental data: one-bolt specimens

3.3.2 Steel-FRP connections

Zafari *et al* (2016) decided to investigate the structural performance of RIBJ for pultruded FRP material concerning its static and fatigue performance. This study was carried out following the guidelines found in *ECCS Publication no. 79* and in standard EN 1090-2:2008. In the specimen's geometry definition not only was this previous European standard taken into account, but also the ASCE pre-standard (Pre-Standard for LRFD, 2010) for the design of pultruded structures. Figures 3.18 and (a) and (b) present a scheme of the two specimen types having M16 or M20 bolting, respectively. Each has two double-lap shear joints with two bolts. For Type 1 specimens (M16 bolting), there is a 2 mm clearance while for Type 2 specimens (M20 bolting) there is 2.4 mm. Specimen's plates were cut from either a wide flange section of size 254×254×9.53 mm or a flat sheet of 6.35 mm thickness.

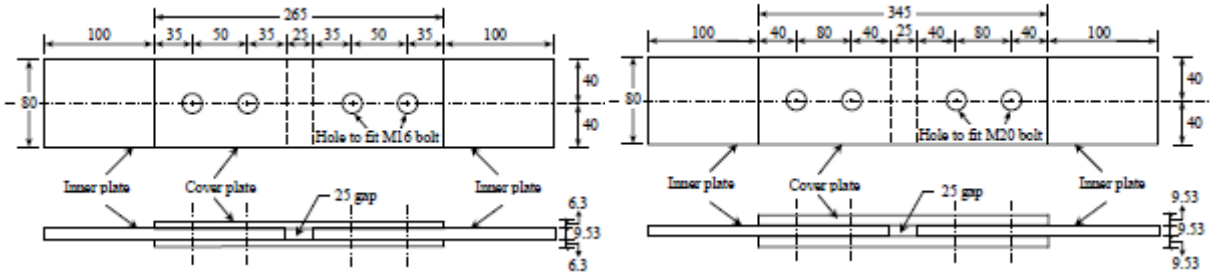

(a) (b)

Figure 3.16 – Geometry of the tested specimens: a) Type 1 specimens; b) Type 2 specimens (dimensions in mm) (Zarafi *et al*, 2016)

All bolts were subjected to a clamping stress produced by a torque of 80 N.m for Type 1 specimens and 88 N.m in the case of Type 2 specimens. The selected structural adhesive was, once again, epoxy based resin Sikadur®-30. However, for some specimens, RenGel® SW 404 was used instead. This is also an epoxy based adhesive which stands out for its hardness and good chemical resistance.

The test procedure to determine slip and fatigue performance of RIBJ is composed of an initial incremental static part and then a cyclic loading. Consequently, specimens were firstly incrementally loaded under static tension until its serviceability design load was reached and posteriorly they were subjected to two million fatigue cycles, at a frequency of 2 Hz. Tests were performed under a constant stress ratio equal to 0.1.

The obtained results were plotted in the form of displacement – log time in order to compare it with the displacement limit, 0.3 mm, caused during the design life of a steel/aluminium structure (which can be as long as 50 years) proposed in Annex G of EN 1090-2:2008. Promising results were obtained since when the three different pultruded FRP specimens (M16 Sikadur, M16 RenGel and M20 RenGel) were subjected to the assumed service load, they presented displacements between 0.04 and 0.09 mm for two million cycles. Therefore, the displacement limit of 0.3 mm for application in steel/aluminium structures may be too conservative for FRP.

The explanation advanced by the paper's authors is related to the existence of viscoelastic properties that characterizes polymeric materials. Moreover, when RIBJ specimens were tested up to four million cycles, with a maximum tension up to 60% of the strength of the standard bolt configuration, no fatigue failure was observed. More tests are required to establish a reliable design method for structures with these new materials.

4 NUMERICAL APPROACH

4.1 Introduction

This chapter presents fatigue numerical modelling of steel connections using standard bolts and resin-injected bolts. As before stated in chapter 2, fatigue life of structural details result from the sum of the endured number of cycles on fatigue crack initiation and propagation phases. The fatigue model to be adopt for bolted connections with resin-injected bolts was performed with the assumption that resin assumes certain cyclic properties with significant contribution in the cracks initiation phase. Resin will interact with the plate hole walls and with the bolt surface, leading to an increase in monotonic and fatigue resistance of the connection.

The procedure adopted for fatigue life prediction was stated in chapter 2.3.5. It establishes that fatigue life prediction for crack initiation period can be performed based on strain-life relations while for crack propagation period the theory of LEFM should be implemented. The transition between these two phases is usually defined through a crack characteristic dimension. In general, the adopted values for this parameter vary between 0.25 and 1 mm, thus several values should be tested in order to find out which value represents better the experimental data.

After characterization of each phase in fatigue damage phenomenon, it is intended to obtain a global prediction on the fatigue behavior of bolted connections using standard bolts or resin-injected bolts. This fatigue life prediction method was implemented on the single shear bolted connections tested by De Jesus *et al* (2010) in which Trezói bridge material was used.

4.2 Fatigue characterization of Trezói bridge material

Previous studies on cyclic elastoplastic behaviour of Trezói bridge material can be found in literature. Correia (2008) performed fatigue researches on laboratory specimens under strain controlled conditions (R_ε = -1) following the guidelines of ASTM E606-92 Standard. The obtained experimental data was then used for definition of the cyclic curve of the material, expressed by the mathematical relation proposed by Ramberg and Osgood – see equation (10). The cyclic strain hardening coefficient and exponent, K' and n', assumed the values 821,3 (MPa) and 0.1768, respectively. In Figure 4.1 is illustrated the obtained cyclic curve for the Trezói bridge material.

Concerning the fatigue behaviour analysis of Trezoi bridge material, in the same research work, strain-life relations were implemented, namely, the previous presented Coffin and Mason (7), Basquin (8) and Morrows (9) models. Figure 4.2 presents the obtained strain-life relations using these three relations.

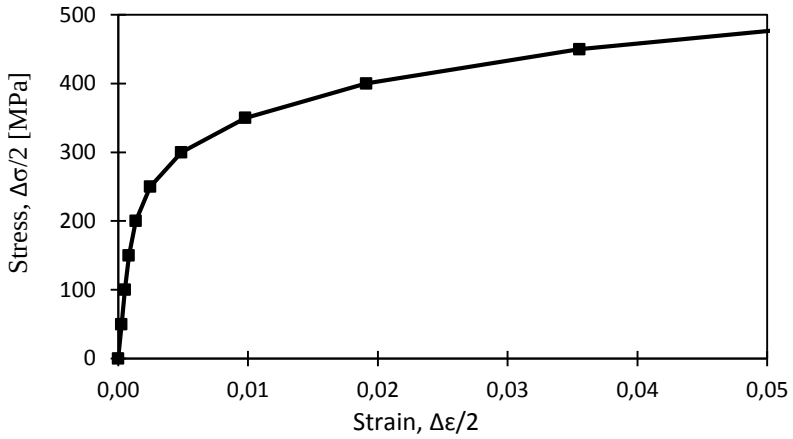

Figure 4.1 – Stress-strain cyclic curve of Trezói bridge material

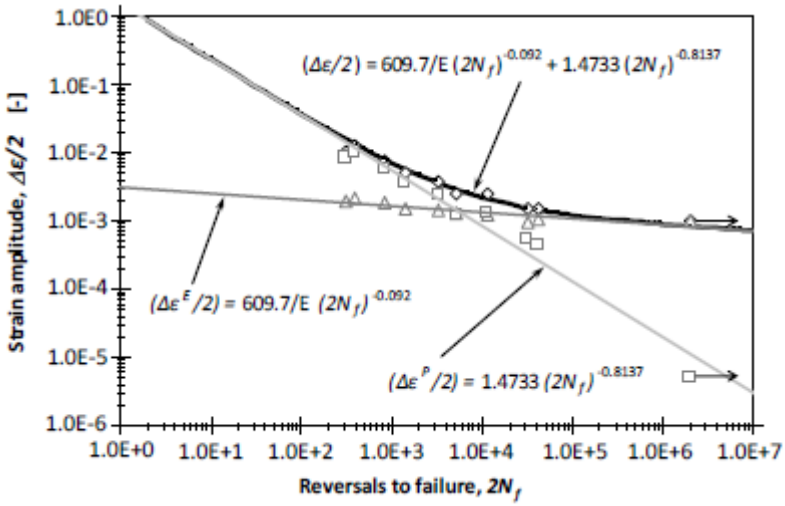

Figure 4.2 – Strain-life curves for the Trezói bridge material (Correia, 2008)

The obtained parameters for the cyclic curve and for the strain-life relation that will be used in the modelling operations are summarized in Table 4.1.

Bridge	K' (MPa)	n' -	σ_f' (MPa)	b -	ε_f' -	c -
Trezói	821,3	0,1768	609,7	-0,092	1,4733	-0,8137

Table 4.1 – Fatigue parameters for modelling the fatigue crack initiation phase.

In order to fully understand the fatigue behaviour of the studied material, the next procedure is to determine the fatigue crack growth rate. Therefore, in Correia (2008), 8 CT specimens (see Figure 2.9 (a)) were produced and tested for three different stress ratios (0, 0.25 and 0.5) according to the ASTM E647-99 Standard. The main objective is to relate the fatigue crack propagation rate, da/dN, with the stress intensity factor range, ΔK, thus the previous standard indicates the mathematical expressions to obtain values for each one. Since the experimental

results presented, approximately, a linear relation between the fatigue crack propagation rate and the stress intensity factor range, the Paris law (20) was chosen to describe experimental data. Therefore, Figure 4.3 shows not only the obtained experimental data for each tested specimen, but also the Paris equation that best represents it with an excellent determination coefficient, R^2=0,93. For this linear equation, constants C and m assume 4.5373×10^{-15} and 3.575, respectively.

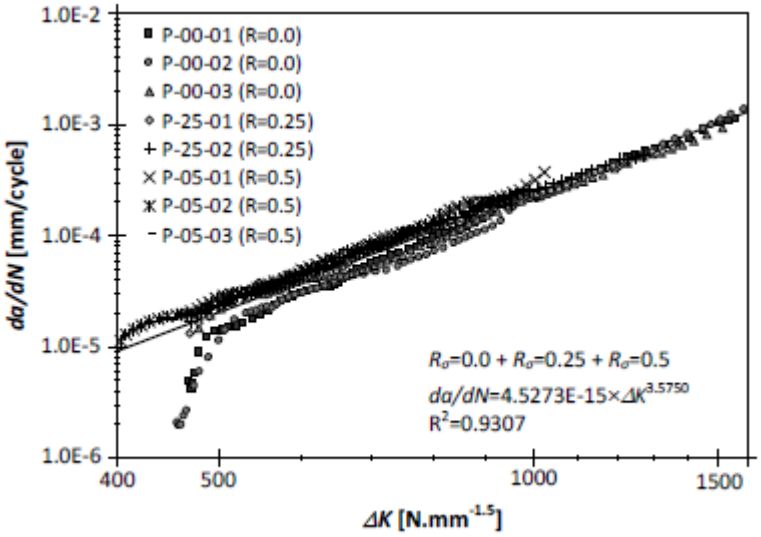

Figure 4.3 – Fatigue crack propagation rate for three different stress ratio (Correia, 2008)

4.3 Finite element modelling

4.3.1 Fatigue crack initiation phase

4.3.1.1 Simulations without resin

Aiming the definition of fatigue crack initiation phase for the studied bolted connection, a 3D finite element model was implemented in Abaqus®. Thus, the parametric model built in this software considers three solids, namely two steel plates and one bolt as shows Figure 4.4. They were modelled with solid linear elements with 8 nodes (C3D8) (ABAQUS, 2014). The constructed model follows the geometry used in the experimental campaign performed by De Jesus *et al* (2010) – see Figure 3.4 (a).

Since the aim of this modelling is to obtain the stress concentration factor (a linear parameter), both plates and bolt were modelled with materials with isotropic and elastic behaviour. Monotonic tensile tests were performed by Correia (2014) on Trezói bridge material following the recommendations of NP EN 10002-1:2006 Standard. The obtained values for the Young modulus and Poisson coefficient were 198.49 GPa and 0.32, respectively. In the case of bolt, these parameters assume 210 GPa and 0.3, respectively, as recommended in NP EN 1993-1-1:2010 for standard steel materials. Although considering materials with linear elastic behaviour, the overall problem is not nonlinear motivated by contact.

In order to implement the same conditions verified on the experimental campaign, the movement of nodes at the end of one plate is restricted in all directions while in the other plate the movement of nodes at its end is restricted only in the directions contained in the plane normal to the loading (YZ plane). In the load direction (X direction) the same nodes are moved 2.5 mm for loading simulation.

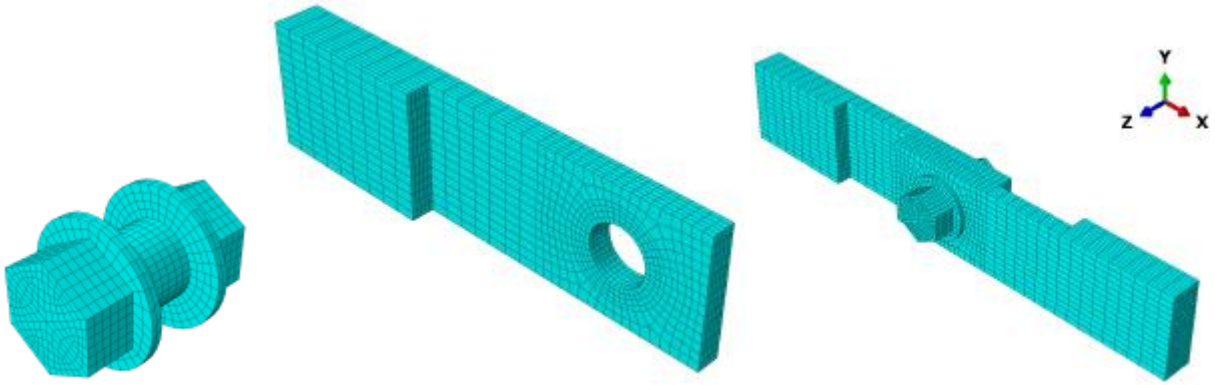

(a) (b) (c)

Figure 4.4 – 3D finite element model withou resin: (a) bolt part; (b) plate part; (c) global model

Contact formulation is influenced by several parameters, such as the contact algorithm, the fiction model, the contact stiffness and the maximum penetration allowed. Between the bolt and plates, contact was modelled using the technology available in Abaqus, namely the surface to surface discretization method. Firstly, contact pairs were defined taking into account the concept of master and slave surfaces. The algorithm establishes that nodes on the slave surface cannot penetrate the segments that make up the master surface while no restrictions are placed for the penetration of master nodes in the slave surface as shown in Figure 4.5. Consequently, slave surface should be the more refined surface (ABAQUS Documentation@, no date).

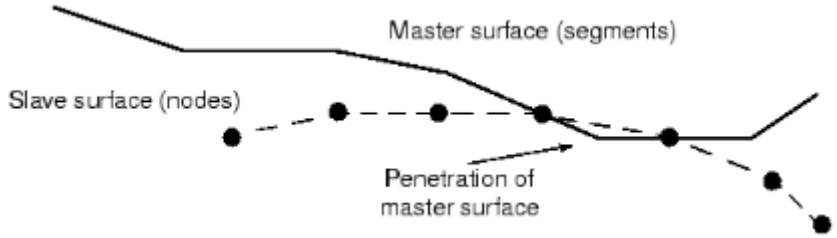

Figure 4.5 – Master – slave formulation (ABAQUS Documentation@, no date)

Furthermore, normal behaviour of contact surfaces is ruled with the Augmented Lagrange algorithm available in the software. It requires the definition of stiffness scale factor (SSF) along with the relative penetration tolerance (RPT). The adopted value for SSF should correspond to a balance between high values that lead to convergence problems in the contact algorithm and very low values which can lead to high penetration and inaccurate solutions.

Normally this parameter assumes values within the range 0.01-1.0. Similar studies can be found in literature where the influence of SSF parameter on the stress concentration factor was studied (Correia, 2008 and Silva, 2009). While Correia (2008) conclude that using SSF equal to 1.0 in a riveted connection lead to a consistent reduction on K_t with the increase in the applied preload, Silva (2009) show that adopting SSF equal to 0.1 is the best option for riveted and bolted connections. Therefore, two values for SSF were implemented: 0.1 and 1.0. Concerning RPT, it establishes the maximum value allowable for penetration (RPT × thickness of the elements underlying the contact surfaces). As standard practice, RPT assumes values within the range 0.01-0.1. Usually this parameter is fixed with the value 0.1. (Correia, 2008 and Silva, 2009).

Concerning sliding formulation of contact surfaces, Abaqus has two options: finite-sliding formulation and small-sliding formulation. As presented in Figure 4.6, in the first option the interaction is updated using the true representation of master surface, while if small-sliding formulation is used, it generates a planar representation of master surface per slave node based on its initial configuration. Finite-sliding formulation has a general applicability whereas small-sliding is normally used to reduce the solution cost. Consequently, in order to reduce the computational cost, all contact pairs were modelled with small-sliding formulation.

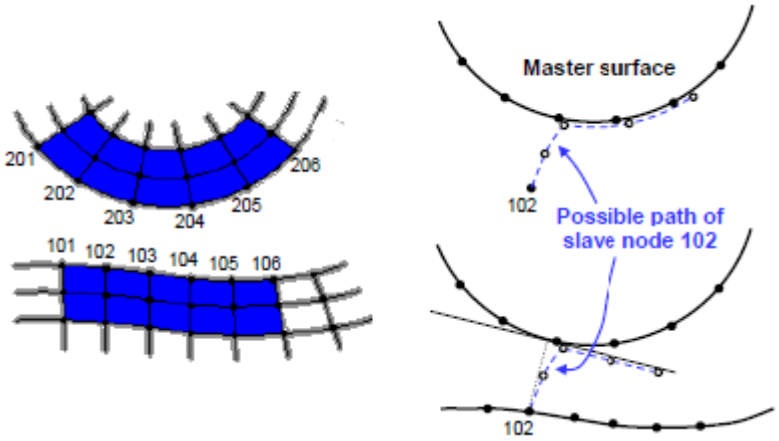

Figure 4.6 – ABAQUS sliding formulation (King and Richards, 2013)

Tangential behaviour of contact surfaces is mainly influenced by the friction coefficient. Similar studies were found in literature which revel that this coefficient influence the obtained results for K_t (Matos *et al*, 2010). However, taking into account that this study is a preliminary approach to the problem, a fixed value was adopted for the friction coefficient. Within the common values adopted in literature for modelling bolted and riveted joints are 0.3 and 0.6 (Imam *et al*, 2007). In the present work, the friction coefficient is equal to 0.3.

There are five contact pairs in this model: between the bolt head and the upper plate surface (contact 1), between the bolt nut and the lower plate surface (contact 2), between the bolt shank and the upper plate hole (contact 3), between the bolt shank and the lower plate hole (contact 4) and between the upper plate surface and the lower plate surface (contact 5). Since plates

mesh are more refined than bolt mesh, in the defined contact pairs, plate surfaces behave as slave surfaces.

Since in the experimental campaign bolts were preloaded using a torque of 80 N.m, modelled bolts were also subjected to an equivalent clamping stress. The relation between the applied torque, M_p, and the preload, $F_{p,C}$, is shown in equation (40) where C_P is a parameter related to the friction behaviour of preloaded surfaces which normally varies between 0.16 and 0.20 (EN 1090-2:2008) and d_b is the bolt diameter. Therefore, assuming the mean value for C_P, the obtained preload, $F_{p,C}$ is equal to 20.2 kN. This preload is introduced in the model by splitting the bolt body in two equal parts and pushing each segment towards the other through the defined preload according its main axis (Montgomery, 2008).

$$F_{p,C} = \frac{M_p}{C_P \cdot d_b} = \frac{80 \cdot 10^{-3}}{0.18 \cdot 0.022} = 20.2\ kN \tag{40}$$

However, in order to take into account possible reductions through the time on the preload magnitude, the influence of decreasing 30% on the applied preload was also studied. The same reduction value is considered in NP EN 1993-1-8:2010 when is intended to calculate the design value for the applied preload on bolts.

Figure 4.7 presents the stress field in the load direction, σ_x, on plates. It shows that stress extreme values are observed in the holes and the stress distribution along the thickness is not uniform with its maximum near the shear plane. Tested models differ in the magnitude of the applied preload and in the contact parameters (SSF and RPT), however they do not present significant changes on the obtained stress fields.

The parameter needed for fatigue life prediction on the initiation phase, the stress concentration factor, K_t, was obtained through equation (41) where $\sigma_{x,peak}$ and $\sigma_{x,nom}$are the maximum and nominal stresses in the load direction, respectively, W is the width of the plate, d_h is the hole diameter, t is the thickness of the plate and F is the applied load.

Table 4.2 presents the obtained values of K_t, the applied load, F (resulted from the displacement) along with the nominal and maximum stresses in the hole section. It shows that the applied preload has influence on the stress concentration factor whereas the contact parameter did not. As was expected, the reduction on the applied preload leaded to higher stress concentrations in the hole. In preloaded bolted connections, load transmission is performed firstly by friction between the connected plates. When friction is not able to withstand the applied load, only then bolts will be subjected to shear load (Silva and Santiago, 2003).

$$K_t = \frac{\sigma_{x,peak}}{\sigma_{x,nom}} = \frac{\sigma_{x,peak}(W - d_h)t}{F} \tag{41}$$

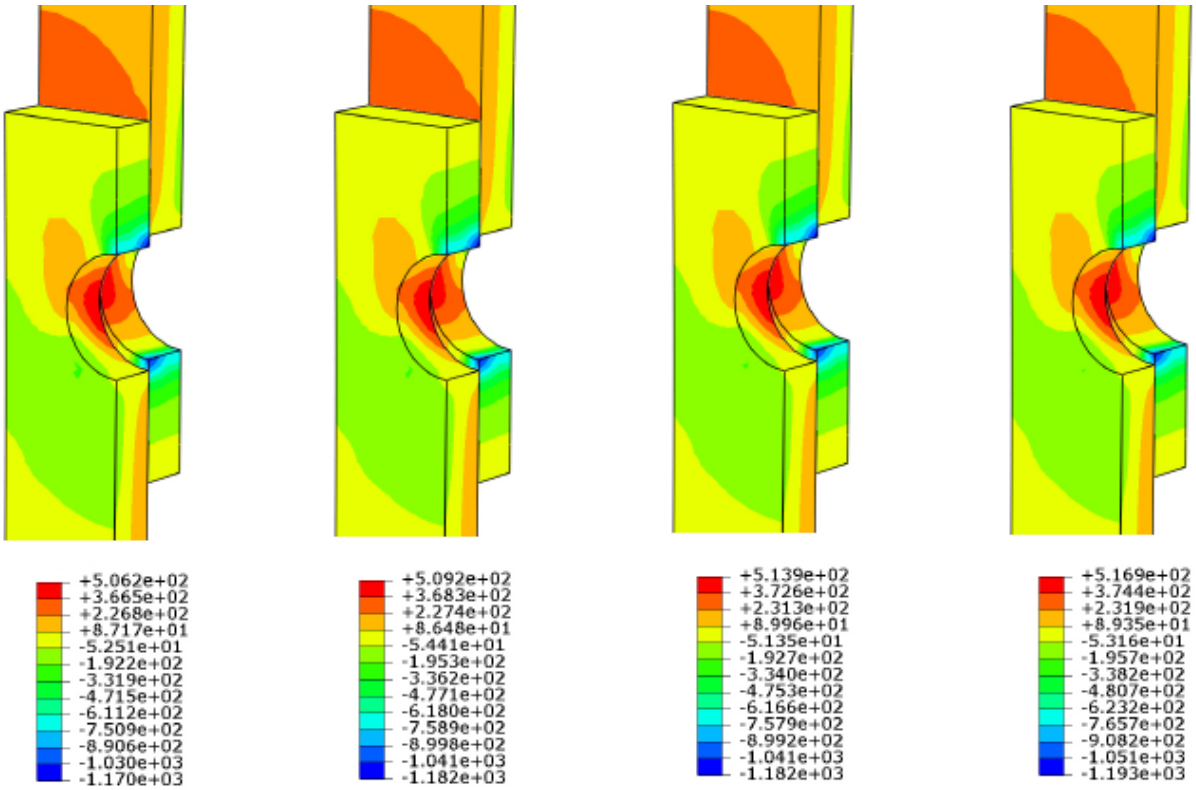

(a) (b) (c) (d)

Figure 4.7 – Stress field on the load direction (MPa): (a) $F_{p,C}$=20.2 kN and SSF=0.1; (b) $F_{p,C}$=20.2 kN and SSF=1.0; (c) $F_{p,C}$=14.1 kN and SSF=0.1; (d) $F_{p,C}$=14.1 kN and SSF=1.0

		F (N)	$\sigma_{x,nom}$ (MPa)	$\sigma_{x,peak}$ (MPa)	*Kt*
$F_{p,C}$ = 20,2 kN	SSF=0,1	55021,5	183,4	506,2	2,76
	SSF=1,0	55353,4	184,5	509,2	2,76
$F_{p,C}$ = 14,1 kN	SSF=0,1	54438,6	181,5	513,9	2,83
	SSF=1,0	54776,3	182,6	516,9	2,83

Table 4.2 – Obtained parameters in simulations without resin

4.3.1.2 Simulations with resin

For fatigue crack initiation analysis when injected bolts are used, the finite element model includes the same three solid elements presented in simulations with standard bolts (two plates, and one bolt) and the resin element. As illustrated in Figure 4.8, resin was modelled in two parts disregarding the shear strength of resin. Finite elements used for resin were also linear solid elements with 8 nodes (C3D8). These resin elements have 1 mm of thickness and they were assembly in the model between the bolt shank and the plates hole walls.

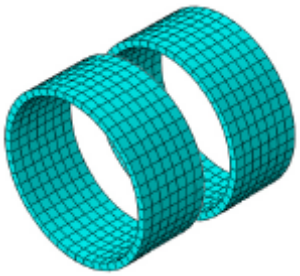

Figure 4.8 – 3D finite element model of resin

This finite element model of resin is intended to be representative of epoxy resin, Sikadur®-30 implemented in the referred experimental campaign. Through previous investigation on literature, it has been studied and tested only for its monotonic properties (Queirós, 2009 and Carvalho, 2013). Since it presents low strength qualities in shear and tensile loading (especially when compared with steel) – see Table 3.1, it is assumed that resin only behaves in compression. Therefore, a plasticity model was considered with a hypothetical isotropic hardening law as shows Figure 4.9. This hardening law intend to simulate the hardening densification of the material which occurs in practice since it is confined inside the connection assembly (Carvalho, 2013). As presented before, Sikadur-30 presents a Young modulus equal to 9.6 GPa in compression and a Poisson ratio equal to 0.26 (Carvalho, 2013).

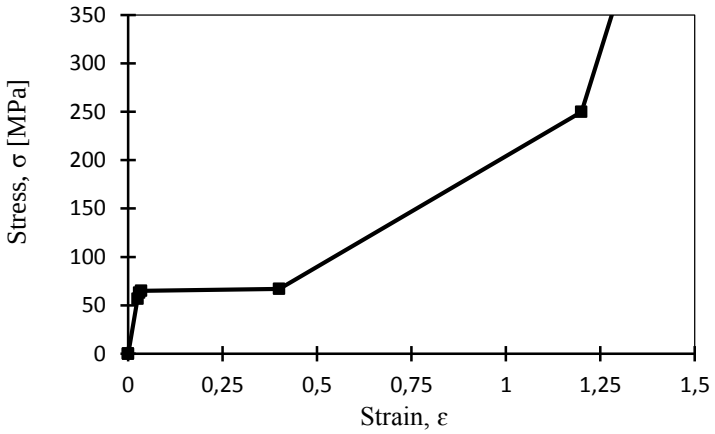

Figure 4.9 – Compression hypothetical hardening law of resin (Carvalho, 2013)

In this model, boundary conditions are equal to the previous model without resin as was the preload magnitude. Previous researches on the fatigue behaviour of bolted connections with adhesives, namely through finite element analysis, have shown that adhesive failure will occur (He, 2011). Therefore, in the contact formulation between resin and steel, separation will be allowed. Once resin has a more refined mesh their surfaces were assumed as slave surfaces. There are nine contact pairs in this model. From the previous model, contact 1, 2 and 5 are maintained. New contact pairs are: between the bolt head and resin (only normal behaviour), between the bolt nut and resin (only normal behaviour), between the lower part of resin and the lower plate, between the upper part of resin and the upper plate, between the lower part of resin

and the bolt shank, between the upper part of resin and bolt shank and between the two resin parts (only normal behaviour).

Figure 4.10 presents the stress field in the load direction, σ_x, on plates of simulations with resin. As in the previous case, stress extreme values are observed in the holes and the stress distribution along the thickness is not uniform with its maximum near the shear plane. Tested models differ in the magnitude of the applied preload and in the contact parameters (SSF and RPT), however there are no significant changes on the obtained stress fields. Following equation (41), the stress concentration factor, K_t, was obtained for each tested case as presented in Table 4.3. It also shows the applied load, F (resulted from the displacement) along with the nominal and maximum stresses in the hole section. The use of resin leaded to constant values of K_t either by reducing the applied preload or changing the contact parameter. However, this fact need more validation especially due to the assumptions in the resin material behaviour.

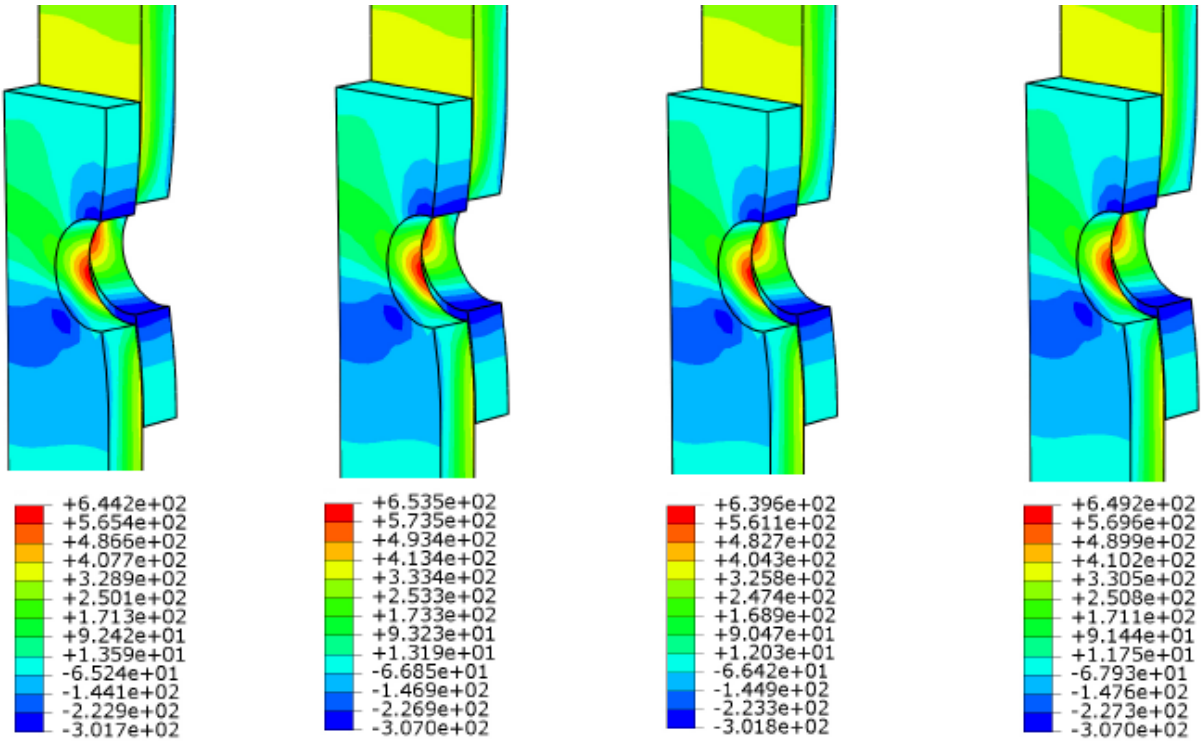

(a) (b) (c) (d)

Figure 4.10 – Stress field on the load direction (MPa): (a) $F_{p,C}$=20.2 kN and SSF=0.1; (b) $F_{p,C}$=20.2 kN and SSF=1.0; (c) $F_{p,C}$=14.1 kN and SSF=0.1; (d) $F_{p,C}$=14.1 kN and SSF=1.0

		F (N)	$\sigma_{x,nom}$ (MPa)	$\sigma_{x,peak}$ (MPa)	Kt
$F_{p,C}$ = 20,2 kN	SSF=0,1	79408,7	264,7	644,2	2,43
	SSF=1,0	80673,8	268,9	653,5	2,43
$F_{p,C}$ = 14,1 kN	SSF=0,1	79109,5	263,7	639,6	2,43
	SSF=1,0	80412	268,0	649,2	2,42

Table 4.3 - Obtained parameters in simulations with resin

4.3.2 Fatigue crack propagation phase

Once fatigue crack initiation phase is studied, the following step is characterizing the next phase in the fatigue damage process – crack growing phase. As mentioned before, crack growth is manly influenced by the material properties of steel plates, thus it is assumed that resin has no influence at this stage. Therefore, previous studies on steel connections constructed with Trezói bridge material were consulted.

In Correia (2008) was studied the crack propagation phase in a riveted steel connection made of material from Trezói bridge and the plate's geometry used was the same as in the present work. In order to obtain the stress intensity factor, finite element models were constructed with several crack lengths and the modified virtual crack closure technique (Krueger, 2002) was implemented.

In this reference work, preload was simulated with a temperature range, ΔT, and using orthotropic thermal expansion properties on the rivet. Numerical data was fitted to sixth grade polynomials in the form of $K = K(a)$ which were used in the integration of Paris law - see equation (26). For the studied case where ΔT is equal to 75ºC (which is equivalent to 22,5 kN) the evolution of the average value of stress intensity factor is presented in equation (41) as a function of crack length.

$$\frac{K}{\sigma} = -0.00001964 \cdot a^6 + 0.00131451 \cdot a^5 - 0.03022960 \cdot a^4 + 0.32870110 \cdot a^3 - 1.78659362 \cdot a^2 + 4.99217777 \cdot a - 0.55179228 \quad (42)$$

4.4 Results analysis

Following the procedure adopted for fatigue life prediction in crack initiation phase (see chapter 2.3.5), local elastoplastic analysis was implemented using the analytical Neuber approach together with the cyclic curve of the material from Trezói bridge stated in Figure 4.1. In the case of simulations without resin, the stress concentration factor adopted for fatigue life prediction was the mean value of the four analysis, K_t=2.80, while for the resin model, K_t=2.43. Then, with the application of the strain-life relation evolved by Morrow – see equation (27) – and the cyclic properties of the same material, the predicted curve for crack initiation is determined.

The prediction of crack propagation phase was based on two initial crack lengths a_i=0.35 mm and a_i=0.30 mm. The increments in the crack length to perform the integration of crack propagation law assumed the value 0.1 mm – see equation (31).

Figures 4.11 and 4.12 shows predicted crack initiation and crack propagation phases together with experimental data for bolted connection with standard bolts and resin-injected bolts, respectively.

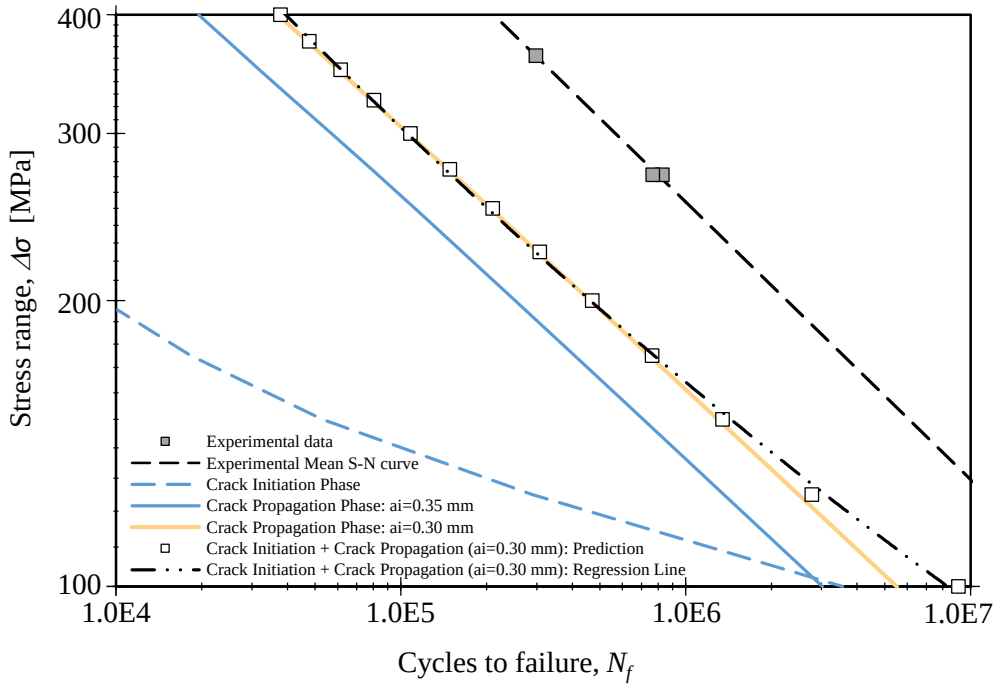

Figure 4.11 – Fatigue life prediction for bolted connections with standard bolts

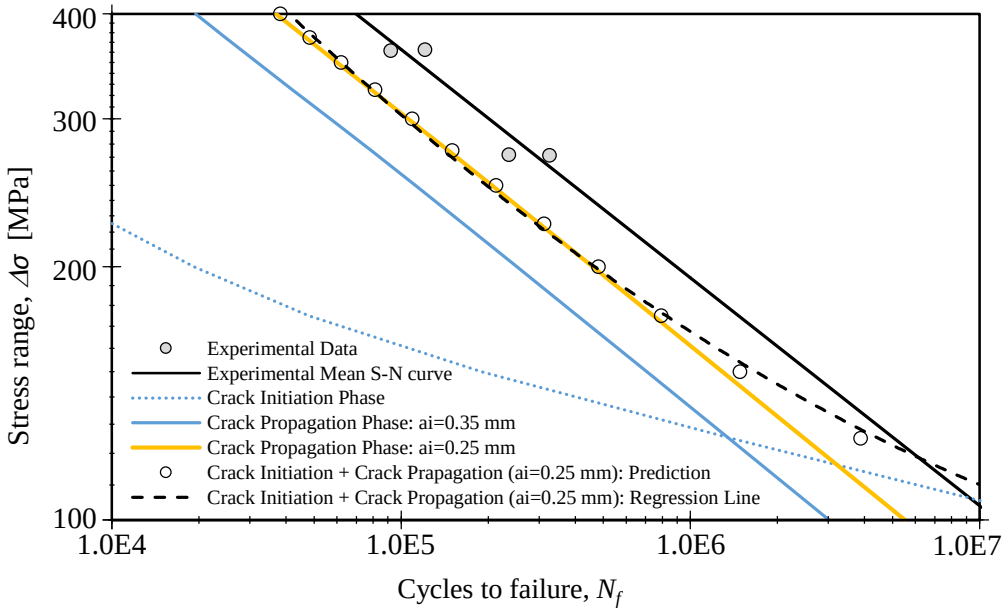

Figure 4.12 – Fatigue life prediction for bolted connections with resin-injected bolts

Finally, in Figure 4.13, experimental data and numerical predictions are presents for bolted connections with standard bolts and injected bolts together in order to establish a comparison between the obtained results.

From these three graphs, results showed that the fatigue prediction model based on two phases together with the characteristic length of a_i=0.30 mm are the most consistent with fatigue experimental data. The obtained S-N curves for crack initiation phase present a smaller slope when compared to the experimental data. However, in the case of S-N curves for crack propagation phase, they are parallel to the experimental data. Another evidence is that predicted global S-N curves are close to the crack propagation curve in low-cycle fatigue regimes since below 1 million cycles these curves are overlapping. For long duration test (high cycle fatigue) the influence of crack initiation curve is evident only for resin-injected bolted connections.

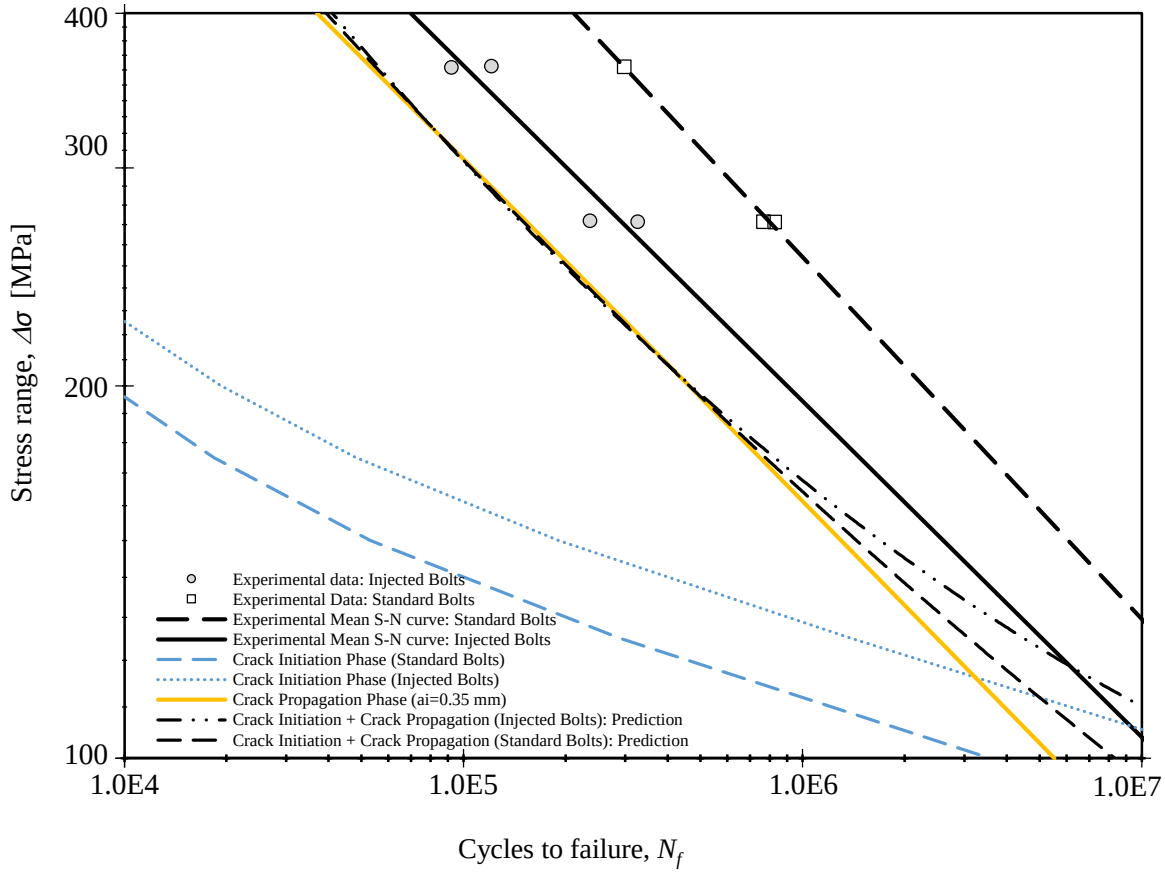

Figure 4.13 – Fatigue life prediction: comparison between bolted connection with standard bolts and resin-injected bolts

Despite predicted crack initiation curve only influence the global curve for high-cycle fatigue, Figure 4.13 shows that bolted connections with resin-injected bolts present better results in crack initiation phase. This fact strengthen the assumption mentioned before in which the presence of resin between the bolt shank and the plate hole walls lead to significant contribution in the crack initiation phase. However, it must be mentioned that the present study performed for the determination of stress concentration factor is a preliminary study since it can be influenced by the nonlinearities of the model, such as contact (friction coefficient influence) and resin. Together with a cyclic characterization of the used adhesive, a fully elastoplastic finite element analysis should be implemented.

5 CONCLUSIONS

In the present work, bolted connections were studied concerning its fatigue behaviour. Namely, bolted connections using standard bolts were compared to bolted connections with adhesives in order to find out which effects the adhesive will produce on the fatigue behaviour of joints. The main conclusions of the present study can be summarized as follows:

- The study of fatigue experimental results for bolted connections found in literature showed that using resin-injected bolts leaded to a consistent fatigue life reduction. However, not only the number of tested specimens was small but also a significant scatter was observed. Regarding bolted connections with bonded plates, fatigue data showed that the use of adhesives helped to transfer the load between the plates and the bolt, leading to an increase in the fatigue strength, notwithstanding when the number of bolts were reduced, the adhesive was unable to maintain the fatigue strength.

- The implemented statistical treatment in the fatigue experimental data allow the definition of a design curve for the studied connections. This proposed design curves can serve as alternative to S-N curves presented in EC3-1-9 which present conservative values especially for high-cycle fatigue.

- Simulations with and without resin were able to represent properly the stress concentration in the hole plates since maximum stress values were observed in the holes. There was not a uniform stress distribution along the thickness of the plates.

- The implemented reduction on the applied preload leaded to higher values for the stress concentration factor.

- K_t parameter presented a constant value for the resin model either by reducing the applied preload or changing the contact parameter. However, the effect of the friction coefficient along with a fully characterization of cyclic properties of resin should be performed.

- Results showed that the fatigue prediction model based on two phases together with the initial characteristic length of a_i=0.30 mm are the most consistent with fatigue experimental data which are within the practices assumed in the literature (a_i from 0.25 to 1 mm for metals).

- Obtained S-N curves for crack initiation phase present a smaller slope when compared to the experimental data, whereas for crack propagation phase, they are almost parallel.

- Results showed that fatigue crack propagation phase is dominant in low-cycle fatigue whereas fatigue crack initiation phase rules in high-cycle fatigue.

6 FUTURE WORKS

As proposals for future works are suggested:

- Implement a deeper study on various modelling parameters which may affect the obtained values of the stress concentration factor, namely the friction coefficient.

- Perform a mesh convergence study on models. This can be done by relating the mesh refinement with the obtained maximum stress in order to obtain the optimum finite element mesh.

- Study the influence on the obtained stress fields of using more complex finite elements.

- Perform a fully elastoplastic finite element analysis in order to overcame the disadvantages of the simplified approach of using the linear parameter, K_t.

- Implement an experimental campaign on several structural adhesives, namely Sikadur®-52, aiming the characterization of its cyclic elastoplastic properties.

Recently, an experimental campaign has been prepared in double and single shear connections in order to assess fatigue resistance when using injected bolts in comparison to standard bolts. Specimens will be constructed with plates with standard steel as well as steel plates manufactured from Eiffel bridge material, a centenary highway and roadway bridge in Viana do Castelo, Portugal. This experimental program is part of a European research program called PROLIFE – Prolonging life of old steel and steel-concrete bridges.

REFERENCES

ABAQUS/CAE User's Guide – Version 6.14 (2014). Dassault Systèmes Simulia Corp., Providence, RI, USA.

ABAQUS Documentation@ (no date). https://www.sharcnet.ca/Software/Abaqus610/Documentation/docs/v6.10/books/gsk/default.htm?startat=ch12s03.html (July 24th, 2016)

Albrecht P., Sahli A., Crute D., Albrecht Ph. and Evans B. (1984) "Application of Adhesives to Steel Bridges. Report No. FHWA/RD-84/073, Federal Highway Administration, McLean, Va., USA.

Alves, A., Sampayo, L., Correia, J., De Jesus, A., Moreira, P. and Tavares, P. (2015) "Fatigue Life Prediction Based on Crack Growth Analysis Using an Equivalent Initial Flaw Size Model: Application to a Notched Geometry". 1st International Conference on Structural Integrity. No. 114. pp. 730-737.

Akesson, B. (1994). "Fatigue Life of Riveted Railway Bridges". PhD Thesis, Chalmers University of Technology, Sweden.

ASCE (2010) "Pre-standard for Load and Resistance Factor Design (LRFD) of pultruded Fiber Reinforced Polymer (FRP) structures" American Composites Manufactures Association.

ASTM (2004). "Standard Specification for High-Strength Low-Alloy Structural Steel". A588, American Society for Testing and Materials, USA.

ASTM (1999). "Standard Test Method for Measurement of Fatigue Crack Growth Rates". E647-99 Vol. 03.01, West Conshohocken, PA, pp. 591-629.

ASTM (1998). "Standard Practice for Statistical Analysis of Linear or Linearized Stress-life (S-N) and Strain-life (ε-N) Fatigue Data" E 739-91., USA.

ASTM (1998). "Standard Practice for strain controlled fatigue testing". E606-92, USA

Basquin, O., (1910). "The Exponential Law of Endurance Tests". Proceedings of the American Society for Testing and Materials, Vol. 10, pp. 625-630.

Benden, S., Abdullah, S. and Ariffin, A. (2009). "Review of Fatigue Crack Propagation Models for Metallic Components". European Journal of Scientific Research, Vol. 28, No. 3, pp. 364-397.

British Standards Institution. (1980). "Steel, concrete and composite bridges: Part 10: Code of practice for fatigue. BS 5400: Part 10, London.

Carvalho, B. (2013) "Modelação por Elementos Finitos do Comportamento de Ligações Aparafusadas Sem e Com Resina Injectada" Dissertação de Mestrado, Departamento de Engenharias da Universidade de Trás-os-Montes e Alto Douro, Vila Real.

Castillo, E. and Fernández-Canteli, A. (2014) "Obtaining S-N curves from crack growth curves: an alternative to self-similarity". International Journal of Fracture. No. 187. pp. 159-172.

Cavadas, F. (2008). "Monitorização e Análise do Comportamento de Pontes Metálicas Antigas – A Ponte Eiffel". Dissertação de Mestrado, Departamento de Engenharia Civil, Universidade do Porto, Portugal

CEN (2010). "Projecto de estruturas de aço. Parte 1-9: Fadiga". NP EN 1993-1-9, Comité Europeu de Normalização, Bruxelas.

CEN (2008) "Execution of steel structures and aluminium structures – Part 2: Technical requirements for steel structures" EN 1090-2. European Committee for Standardization Brussels.

Coffin, L. (1954). "A Study of the Effects of the Thermal Stresses on a Ductile Metal". Translations of the ASME, Vol. 76, pp. 931-950.

Correia, J., Blasón, S., De Jesus, A., Canteli, A., Moreira, P. and Tavares, P. (2016) "Fatigue Life Prediction Based on na Equivalente Initial Flaw Size Approach and a New Normalized Fatigue Growth Model" Engineering Failure Analysis. http://www.sciencedirect.com/science/article/pii/S1350630716301261

Correia, J. (2014). "An Integral Probabilistic Approach for Fatigue Lifetime Prediction of Mechanical and Structural Components". PhD Thesis, Faculty of Engineering of the University of Porto, Porto.

Correia, J., De Jesus, A. and Fernández-Canteli, A. (2013) "Local Unified Probabilistic Model for Fatigue Crack Initiation and Propagation: Application to a notch geometry". Engineering Structures 52. pp. 394-407.

Correia, J. (2008). "Desenvolvimento de Modelos de Previsão da Vida à Fadiga de Ligações Rebitadas". Dissertação de Mestrado, Departamento de Engenharias da Universidade de Trás-os-Montes e Alto Douro, Vila Real.

De Jesus, A., Silva, A. and Correia, J. (2014) "Fatigue of Riveted and Bolted Joints Made of Puddled Iron - A Numerical Approach" Journal of Construction Steel Research, No. 108, pp. 164-177.

De Jesus, A., Silva, J., Figueiredo, M., Ribeiro, A., Fernandes, A. and Correia, J. (2010). "Fatigue Behaviour of Resin-Injected Bolts: An Experimental Approach". Iberian Conference on Fracture and Structural Integrity, Porto.

De Jesus, A., Silva, A., Figueiredo, M., Correia, J., Ribeiro, A. and Fernandes, A. (2010). "Strain-life and Crack Propagation Fatigue Data from Several Portuguese Old Metallic Riveted Bridges". Engineering Failure Analysis, No. 18, pp. 148-163.

Dowling, N. and Begley, J. (1976) "Fatigue Crack Growth During Gross Plasticity and the J-integral". Mechanics of Crack Growth. ASTM STP 590, PA, pp. 82-105. Philadelphia

ECCS (1994). "European Recommendations for Bolted Connections with Injection Bolts". Publication No. 79.

Ellyin, F. and Kujawski D. (1986) An Energy-based Fatigue Failure Criterion. Microstructure and Mechanical Behaviour of Materials, Vol. II, EMAS, West Midlands, UK.

Fernandes, A., De Jesus, A., Silva, A. and Correia, J. (2012). "Retrofitting of Old Riveted Portuguese Bridges. Past and Current Remnant Life Assessment Research". 15th International Conference on Experimental Mechanics, Porto

Forman, G. (1972). "Study of Fatigue Crack Initiation from Flaws Using Fracture Mechanics Theory. Engineering Fracture Mechanics, 4(2), pp. 333–345.

Gresnigt, A., Sedlacek, G. and Paschen, M. (2000). "Injection bolts to repair old bridges" (https://www.researchgate.net/publication/237456449_INJECTION_BOLTS_TO_REPAIR_OLD_BRIDGES) (June 16th, 2016).

Gresnight, A. and Stark, J. (1996) "Design of bolted connection with injection bolts" Connections in Steel Structures III: Behaviour, Strength and Design. pp. 77-87.

Hartman. A. and Schijve J. (1970) "The Effects of Environment and Load Frequency on the Crack Propagation Law for Macro Fatigue Crack Growth in Aluminum Alloys". Engineering Fracture Mechanics, 1(4), pp. 615-631.

He, X. (2011) "A Review of Finite Element Analysis of Adhesively Bonded Joints" International Journal of Adhesion & Adhesives No. 31. Pp. 248-264

Helmerich, R., Kühn, B. and Nussbaumer, A. (2007) "Assessment of Existing Steel Structures. A Guideline for Estimation of the Remaining Fatigue Life". Structure and Infrastructure Engineering, Vol. 3, No. 3, pp. 245-255.

Imam, B., Righiniotis, T. and Chryssanthopoulos, M. (2007). "Numerical modelling of riveted railway bridge connections for fatigue evaluation", Engineering Structures, 29(11), pp. 3071-3081.

IPQ (2010) "Eurocódigo 3 – Projecto de estruturas de aço. Parte 1-1: Regras gerais e regras para edifícios". NP EN 1993-1-1. Instituto Português da Qualidade

IPQ (2010) "Eurocódigo 3 – Projecto de estruturas de aço. Parte 1-8: Projecto de ligações". NP EN 1993-1-8. Instituto Português da Qualidade

IPQ (2006) "Materiais metálicos. Ensaios de tracção. Parte 1: Método de ensaio à temperatura ambiente. NP EN 10002-1. Instituto Português da Qualidade. Lisboa.

Jorge, R., Ribeiro, A. De Jesus, A., Figueiredo, M., Castro, P. and Fernandes, A. (2006). "Ponte Eiffel - Viana do Castelo. Avaliação de Resultados de Programa Experimental. IDMEC/FEUP: Faculdade de Engenharia, Universidade do Porto.

King, S. and Richards, T. (2013) "Solving Contact Problems with Abaqus" DS UK Ltd, Coventry.

Kortiš J. (2011). "The Numerical Solution of the Bolted Connection with the Low-quality Injected Bolts". Proceedings of the 9th International Conference on New Trends in Statics and Dynamics of Buildings. Bratislava, Slovakia.

Krueger, R. (2002) "The virtual crack closure technique: history, approach and applications" Technical report, NASA/CR-2002-211628 ICASE Report N.º 2002-10 NASA Langley Research Center Hampton

Kujawski, D. (1989) "Fatigue Failure Criterion Based on Strain Energy Density". Mechanika Teoretyczna I Stosowana.

Larsson, T. (2009). "Fatigue Assessment of Riveted Bridges". PhD Thesis. Lulea University of Technology, Sweden.

Manson, S. (1954). "Behaviour of Materials Under Conditions of Thermal Stress", NACA, Technical Note No. 2933, National Advisory Committee for Aeronautics.

Matos, R., Correia, J., De Jesus, A., Rebelo, C., Silva, L. (2010) "Avaliação da Resistência à Fadiga de Ligações Metálicas Recorrendo aos Modelos de Aproximação Local" Encontro Nacional sobre Conservação e Reabilitação de Estruturas (REABILITAR'10), LNEC, Lisboa

Mattes, J. (2007). "Substituição de Rebites por Parafusos Injectados com Resina". Tese de Mestrado, 180 pag., IST/UTL, Lisboa.

Miravalles, M. (2007). "The creep behaviour of adhesives". Master's Thesis. Chalmers University of Technology, Sweden

Montgomery, J. (2008) "Boundary Condition Influences on Shank Stress in 3D Solid Bolt Simulation". Abaqus User's Conference.

Morrow, J., (1965). "Cyclic Plastic Strain Energy and Fatigue of Metals", Internal Friction, Damping and Cyclic Plasticity, ASTM, STP 378, pp. 45-87.

Neuber, H. (1961). "Theory of Stress Concentration for Shear-Strained Prismatic Bodies with Arbitrary Nonlinear Stress-Strain Law", Translations of the ASME, Journal of Applied Mechanics, Vol. 28, pp. 544-550.

Nikolovski, T. (2009) "Technical information 01: Injection Bolts" https://issuu.com/fakom/docs/ti-01-injectbolts-eng (June 25th, 2016).

Noroozi, A., Glinka, G. and Lambert, S. (2005) "A Two Parameter Driving Force for Fatigue Crack Growth Analysis". International Journal of Fatigue, Vol. 27, pp. 1277-1296.

Paris, P. and Erdogan, F. (1963) "A critical analysis of crack propagation laws.". Trans. ASME, Series D, Vol. 85, pp. 523-535.

Paris, P., Gomez, M. and Anderson, W. (1961) "A rational analytical theory of fatigue.". The Trend of Engineering, Vol. 13, pp. 9-14.

Queirós, E. (2009) "Comportamento de Ligações do Tipo Cavilha Reforçadas com CFRP em Estruturas de Madeira" Dissertação de Mestrado, Departamento de Engenharias da Universidade de Trás-os-Montes e Alto Douro, Vila Real.

Qureshi, J. and Mottram, J. (2012) "Resin injected bolted connections: A step towards achieving slip-resistant joints in FRP bridge engineering" FRP Bridges 2012 Net Composites.

Ramberg, W. and Osgood, W. (1943). "Description of Stress-strain Curves by Three Parameters", NACA Tech. Note No. 902.

Ribeiro, A., Correia, J., Silva, A. and De Jesus, A. (2011). "Evolution of Fatigue History". 21st Brazilian Congress of Mechanical, Natal.

Schijve, J. (2004). "Fatigue of Structures and Materials". Kluwer Academic Publishers, New York.

Sikadur®-30. Product Data Sheet. http://prt.sika.com/pt/solutions_products/document_download_area/construction_download/fichas-de-produto--sika-d.html (June 19th, 2016).

Sikadur®-52. Product Data Sheet. https://prt.sika.com/dms/getdocument.get/99182134-32ad-37e2-a2ca-33bc83235a54/76.%20Sikadur%2052%20Injection_07.608.pdf (June 19th, 2016).

Silva, L., Santiago, A. (2003) "Manual de Ligações Metálicas" Associação Portuguesa de Construção Metálica e Mista, Coimbra

Silva, J. (2009). "Comparação Entre o Comportamento à Fadiga de Ligações Rebitadas e Aparafusadas" Dissertação de Mestrado, Departamento de Engenharias da Universidade de Trás-os-Montes e Alto Douro, Vila Real.

Smith, K., Watson, P. and Topper, T. (1970). "A Stress-Strain Function for the Fatigue of Metals", Journal of Materials, JMLSA, Vol. 5, No. 4, pgs. 767-778.

Walker, K. (1970). "The Effect of Stress Ratio During Crack Propagation and Fatigue for 2024-T3 and 7076-T6 aluminum. In: Effect of environment and complex load history on fatigue life, ASTM STP 462. pp.1–14. Philadelphia.

Zarafi, B., Qureshi, J., Mottram, J. and Rusev, R. (2016). “Static and Fatigue Performance of Resin Injected Bolts for a Slip and Fatigue Resistant Connection in FRP Bridge Engineering” Structures, ISSN.